Supersymmetry, naturalness, and signatures at the CERN LHC

Ryuichiro Kitano[1] and Yasunori Nomura[2,3]

[1]*Stanford Linear Accelerator Center, Stanford University, Stanford, California 94309, USA*
[2]*Department of Physics, University of California, Berkeley, California 94720, USA*
[3]*Theoretical Physics Group, Lawrence Berkeley National Laboratory, Berkeley, California 94720, USA*

Weak scale supersymmetry is often said to be fine-tuned, especially if the matter content is minimal. This is not true if there is a large *A* term for the top squarks. We present a systematic study on fine-tuning in minimal supersymmetric theories and identify low-energy spectra that do not lead to severe fine-tuning. Characteristic features of these spectra are: a large *A* term for the top squarks, small top squark masses, moderately large $\tan\beta$, and a small μ parameter. There are classes of theories leading to these features, which are discussed. In one class, which allows a complete elimination of fine-tuning, the Higgsinos are the lightest among all the superpartners of the standard model particles, leading to three nearly degenerate neutralino/chargino states. This gives interesting signals at the LHC—the dilepton invariant mass distribution has a very small endpoint and shows a particular shape determined by the Higgsino nature of the two lightest neutralinos. We demonstrate that these signals are indeed useful in realistic analyses by performing Monte Carlo simulations, including detector simulations and background estimations. We also present a method that allows the determination of all the relevant superparticle masses without using input from particular models, despite the limited kinematical information due to short cascades. This allows us to test various possible models, which is demonstrated in the case of a model with mixed moduli-anomaly mediation. We also give a simple derivation of special renormalization group properties associated with moduli mediated supersymmetry-breaking, which are relevant in a model without fine-tuning.

I. INTRODUCTION

What is the physics at the TeV scale and how can we test it? These questions become more pressing as we approach the LHC era, which will start within two years. It is extremely important now to consider what we expect to see at these energies, especially because the LHC is a hadron collider experiment, in which relations between experimental data and the underlying theory are not so simple. Knowing what we are looking for would certainly help to identify the physics at the TeV scale and may even be necessary, as the determination of the TeV physics at the LHC and other experiments will most likely take the form of a slow elimination process.

There are already several hints on possible physics at the TeV scale. They come from combining a theoretical criterion of naturalness and precision measurements of electroweak observables and rare flavor- and *CP*-violating processes. Among these, the combination of naturalness and the electroweak data seems to give the most unambiguous hint, because these constraints cannot be satisfied simply by imposing approximate symmetries already present in the standard model gauge and matter sector. Interpreted naively, the precision electroweak data suggest the existence of a light Higgs boson, with the contributions to the electroweak observables from other physics highly suppressed [1]. Naturalness then implies that there must be a new weakly-interacting physics at a TeV scale or below, which cuts off quadratically divergent contributions to the Higgs mass-squared parameter arising from loops of the standard model particles.

Weak scale supersymmetry is an ideal candidate for the new physics. Loops of superparticles cancel the quadratic divergences from those of the standard model particles. The new interactions for the superparticles are necessarily weak, as they are related to the standard model interactions by supersymmetry. Moreover, the mass of the lightest Higgs boson is predicted to be small, $M_{\mathrm{Higgs}} \lesssim 200$ GeV in most (even extended) theories, which is very much consistent with the precision electroweak data. With the introduction of *R* parity and the assumption of flavor universality for the superparticle masses, weak scale supersymmetry can provide a fully consistent framework for physics of electroweak symmetry breaking.

Postulating weak scale supersymmetry alone, however, does not much narrow down signatures at the LHC. Depending on the relative sizes for the soft supersymmetry-breaking parameters, one can have drastically different signatures at the LHC. The number of relatively model-independent signals is also small, making it difficult to discriminate supersymmetry from other TeV-scale physics. A generic signal of weak scale supersymmetry is large missing transverse energy in association with jets and/or isolated leptons. Such a signal, however, arises in almost any theory where the lightest TeV-scale particle is stable and neutral, which is suggested by the existence of the dark matter of the universe. It is then an important task to narrow down the parameter space of weak scale supersymmetry further and to perform a detailed study of the LHC signals there. One of the important goals of such a study is to identify generic signals associ-

ated with a particular parameter region so that the non-observation of those signals will allow us to exclude the region.

How should we choose regions among the huge parameter space of weak scale supersymmetry? An obvious way is to assume a particular supersymmetry-breaking model, such as the minimal supergravity or gauge mediation model, based on the simplicity of the model. This selects a slice in the parameter space of soft supersymmetry-breaking parameters, which depends only on a few free parameters. These studies have been performed by many authors, for example, in [2–8]. In this paper we take a different criterion to choose the region. We use the hint from naturalness to the maximal amount and consider what are generic implications of it on the spectrum of super-particles and on LHC signals. Fortunately, or unfortunately, generic parameter regions of weak scale supersymmetry satisfying existing experimental constraints do not lead to the correct scale for electroweak symmetry breaking without significant fine-tuning. This information, therefore, can be used to constrain the parameter space of soft supersymmetry-breaking parameters and thus to narrow down possible signatures at the LHC. Of course, the input from naturalness alone does not lead to unambiguous signatures in a wide variety of possible supersymmetric theories. In this paper we focus our attention to the case where the matter content at the weak scale is minimal, i.e. given by that of the minimal supersymmetric standard model (MSSM).

What are generic implications of fine-tuning on the spectrum of superparticles in a theory with the minimal matter content? As discussed in Ref. [9], the fine-tuning problem of minimal supersymmetry can be solved without extending its matter content if the trilinear scalar term (A term) for the top squarks is large and the holomorphic supersymmetry-breaking term (μB term) for the Higgs doublets is small. This allows us to evade the LEP II bound on the Higgs boson mass with relatively small superparticle, specifically top squark, masses. Then, if soft supersymmetry-breaking parameters are generated (effectively) at low energies, the sensitivity of the electroweak scale to the fundamental parameters of the theory can be very mild. One of the consequences of such a scenario is that the top squarks are relatively light and have a large mass splitting between the light and heavy ones. Another important consequence is that the Higgsinos are rather light, with the masses smaller than about 190 GeV (270 GeV) for fine-tuning better than $\approx 20\%$ (10%), which is because naturalness requires any contribution to the Higgs boson squared mass to be small, including the supersymmetric contribution. We argue that these features are robust and appear quite generically in a minimal supersymmetric theory without significant fine-tuning.

This argument provides a strong motivation to consider the case in which the lightest neutral Higgsino is the light-

est supersymmetric particle (LSP). While it is not a necessary consequence of solving the supersymmetric fine-tuning problem, the Higgsino LSP in fact arises in a large class of theories in which the pattern of soft supersymmetry-breaking parameters described above is naturally obtained. It is, therefore, quite important to perform an LHC study for the case of the Higgsino LSP and identify possible signatures. An important consequence of the Higgsino LSP scenario is that there are three nearly degenerate neutralino/chargino states, $\tilde{\chi}_1^0$, $\tilde{\chi}_2^0$ and $\tilde{\chi}_1^+$, with $\tilde{\chi}_1^0$ being the LSP. We show that this structure can give interesting signatures at the LHC in the dilepton invariant mass distribution arising from the decay $\tilde{\chi}_2^0 \to \tilde{\chi}_1^0 l^+ l^-$. We discuss in what sense these are characteristic signatures of the Higgsino LSP, and under what circumstances the signals can be used in realistic analyses.

To demonstrate the usefulness of the signatures, we need to choose specific parameter points and perform Monte Carlo simulations, including detector simulations and standard model background. We do this in the model discussed in Refs. [9–11], where the desired pattern of the soft supersymmetry-breaking masses, a large A term and a small μB term, are obtained while evading the existing experimental constraints such as the one from $b \to s\gamma$. We show that the dilepton invariant mass distribution from $\tilde{\chi}_2^0 \to \tilde{\chi}_1^0 l^+ l^-$ is indeed useful to test the Higgsino nature of the LSP and to extract the information on a small mass difference between $\tilde{\chi}_1^0$ and $\tilde{\chi}_2^0$. We also show that important parameters of the model, the overall mass scale and the μ parameter, are determined by various other endpoint analyses. In fact, we show that these parameters are overconstrained, so that we can test some of the model predictions. We perform these analyses for an integrated luminosity of 30 fb^{-1}, but essentially the same conclusion is obtained with 10 fb^{-1}. The technique presented here can also be used in a larger class of theories having similar superparticle spectra.

The organization of the paper is as follows. In Sec. II, we present a systematic study on naturalness in general supersymmetric theories, especially focusing on the case where the matter content at the weak scale is minimal. We give general criteria that natural supersymmetric models with the minimal matter content must satisfy, and present characteristic patterns for the superparticle spectrum arising from these models. In Sec. III, we discuss LHC signals of the Higgsino LSP scenario, which naturally arises in a class of models that do not suffer from fine-tuning. We find that a combination of the endpoint and the shape of the dilepton invariant mass distribution provides a powerful tool to test the scenario. In Sec. IV, we perform Monte Carlo simulations to demonstrate that these signals are indeed useful in a realistic situation. We also present an analysis that allows us to determine the masses of the gluino, squarks, and the two lightest neutralinos in the Higgsino LSP scenario, without relying on details of the underlying model. We

illustrate that these information can be used to test and/or discriminate between possible models. Discussion and conclusions are given in Sec. V. In the Appendix, we give a simple derivation of special renormalization group properties of moduli mediated supersymmetry-breaking models, which are relevant in the model studied in Sec. IV.

II. SUPERSYMMETRY AND NATURALNESS

One of the principal motivations for weak scale supersymmetry is to provide a solution to the naturalness problem of the standard model. This has, however, been put in a subtle position after nondiscovery of both superparticles and a light Higgs boson at LEP II. In a generic parameter region motivated by simple supersymmetry-breaking models, fine-tuning of order a few percent is required to reproduce the correct scale for electroweak symmetry breaking while evading the constraints from LEP II. This problem, called the supersymmetric fine-tuning problem, has attracted much attention recently, and several solutions have been proposed, e.g., in [9,10,12–22]. In this section we reconsider the problem and see what are generic implications of it, especially in the context of theories with the minimal matter content. One of our emphases here is on the fact that the supersymmetric fine-tuning problem may simply be a problem of the supersymmetry-breaking mechanism and not necessarily that of minimal supersymmetry itself.

A. Large A_t and small μB in minimal supersymmetry

We begin our discussion by considering fine-tuning in the Higgs potential in general weak scale supersymmetric theories. Let h be the Higgs field whose vacuum expectation value (VEV) breaks the electroweak symmetry. In minimal supersymmetry, h is a linear combination of the two Higgs doublets, H_u and H_d. The potential for h is given by

$$V = m_h^2 |h|^2 + \frac{\lambda_h}{4} |h|^4, \qquad (1)$$

where m_h^2 is negative and λ_h is positive. By minimizing it, we obtain $v^2 \equiv \langle h \rangle^2 = -2m_h^2/\lambda_h$ and $M_{\text{Higgs}}^2 = \lambda_h v^2$, where M_{Higgs} is the mass of the physical Higgs boson, so that

$$\frac{M_{\text{Higgs}}^2}{2} = -m_h^2. \qquad (2)$$

We thus find that $|m_h^2|$ cannot be large for a light Higgs boson: $|m_h^2|^{1/2} \lesssim 140 \text{ GeV}$ (90 GeV) for $M_{\text{Higgs}} \lesssim 200 \text{ GeV}$ (130 GeV).

What is m_h^2 in supersymmetric theories? For moderately large $\tan\beta \equiv \langle H_u \rangle / \langle H_d \rangle$, e.g. $\tan\beta \gtrsim 2$, m_h^2 can be written as

$$m_h^2 = |\mu|^2 + m_{H_u}^2|_{\text{tree}} + m_{H_u}^2|_{\text{rad}}, \qquad (3)$$

where μ is the supersymmetric mass for the Higgs dou-

blets, and $m_{H_u}^2|_{\text{tree}}$ and $m_{H_u}^2|_{\text{rad}}$ represent the tree-level and radiative contributions to the soft supersymmetry-breaking mass squared for H_u. The dominant contribution to $m_{H_u}^2|_{\text{rad}}$ arises from top-stop loop:

$$m_{H_u}^2|_{\text{rad}} \simeq -\frac{3y_t^2}{8\pi^2}(m_{Q_3}^2 + m_{U_3}^2 + |A_t|^2)\ln\left(\frac{M_{\text{mess}}}{m_{\tilde{t}}}\right), \qquad (4)$$

where y_t is the top Yukawa coupling, $m_{Q_3}^2$ and $m_{U_3}^2$ soft supersymmetry-breaking masses for the third-generation doublet quark, Q_3, and singlet up-type quark, U_3, and A_t the trilinear scalar interaction parameter for the top squarks (our definition for the A parameters is such that a scalar trilinear coupling is given by the product of the Yukawa coupling and the A parameter, e.g., $\mathcal{L} = -y_t A_t \tilde{q}_3 \tilde{u}_3 H_u +$ h.c.). The quantity M_{mess} represents the scale at which squark and slepton masses are generated, and $m_{\tilde{t}}$ the scale of the top squark masses determined by $m_{Q_3}^2$, $m_{U_3}^2$ and A_t. Note that M_{mess} can be an effective scale different from the true scale of scalar mass generation in a case that the theory possesses special relations among various parameters.

For fine-tuning to be absent, each term in the right-hand-side of Eq. (3) should not be much larger than the left-hand-side, which is related to the physical Higgs boson mass by Eq. (2). Let us first consider $m_{H_u}^2|_{\text{rad}}$. The amount of fine-tuning from this term is given by $M_{\text{Higgs}}^2/2m_{H_u}^2|_{\text{rad}}$, so that requiring the absence of fine-tuning worse than Δ^{-1} leads to the condition

$$m_{\tilde{t}}^2 \lesssim \frac{2\pi^2}{3y_t^2} \frac{M_{\text{Higgs}}^2}{(1 + \frac{x^2}{2})\Delta^{-1}\ln\frac{M_{\text{mess}}}{m_{\tilde{t}}}}$$

$$\approx (700 \text{ GeV})^2 \frac{1}{1 + \frac{x^2}{2}}\left(\frac{20\%}{\Delta^{-1}}\right)\left(\frac{3}{\ln\frac{M_{\text{mess}}}{m_{\tilde{t}}}}\right)\left(\frac{M_{\text{Higgs}}}{200 \text{ GeV}}\right)^2, \qquad (5)$$

where we have set $m_{Q_3}^2 \simeq m_{U_3}^2 \simeq m_{\tilde{t}}^2$ for simplicity, and $x \equiv |A_t|/m_{\tilde{t}}$. This has the following implication on the properties of the supersymmetry-breaking sector [18]. Unless M_{mess} is extremely small, e.g. $M_{\text{mess}} \lesssim 10$ TeV, the absence of fine-tuning, defined by $\Delta^{-1} \gtrsim 20\%$, requires $m_{\tilde{t}} \lesssim 700$ GeV, where we have used $M_{\text{Higgs}} \lesssim 200$ GeV as suggested by the precision electroweak data. This implies that a naive low-scale mediation model, leading to the "minimal gauge mediated mass relation" $m_{\tilde{t}}^2/m_{\tilde{e}}^2 \approx g_3^4/g_1^4$, is unlikely to solve the fine-tuning problem because it gives too light right-handed sleptons. For a lighter Higgs boson, we obtain severer bounds on $m_{\tilde{t}}$: for $M_{\text{Higgs}} \simeq 140$ GeV, for example, we find $m_{\tilde{t}} \lesssim 700$ GeV even for $\Delta^{-1} \simeq 10\%$. Note that the condition of Eq. (5) applies independently of any other considerations.[1]

---

[1]In the case that $\ln(M_{\text{mess}}/m_{\tilde{t}})$ is large, for example, in gravity mediated models, the expression in Eq. (4) is not reliable and we should sum up the leading logarithms using renormalization group equations. This case will be addressed in the next subsection.

Light top squarks suggested by Eq. (5) leads to a tension with the LEP II bound on the Higgs boson mass, $M_{\text{Higgs}} \gtrsim$ 114.4 GeV [23], since in the MSSM having M_{Higgs} larger than the Z boson mass, m_Z, requires radiative corrections arising from top-stop loop, which grow with the top squark masses [24]. A simple way to avoid the conflict is to introduce an additional contribution to the Higgs boson mass other than that in the MSSM. An example of such theories can be found in Ref. [18], where the required properties for the supersymmetry-breaking sector are realized by strong gauge dynamics breaking supersymmetry at a scale of $(10 \sim 100)$ TeV. What if we do not introduce any other contribution to M_{Higgs} than that in the MSSM? In this case it is unlikely that M_{Higgs} can be larger than 130 GeV, so Eq. (5) leads to a severer bound

$$m_{\tilde{t}}^2 \lesssim (450 \text{ GeV})^2 \frac{1}{1 + \frac{x^2}{2}} \left(\frac{20\%}{\Delta^{-1}}\right)\left(\frac{3}{\ln\frac{M_{\text{mess}}}{m_{\tilde{t}}}}\right). \quad (6)$$

While this bound is strong, it still leaves a room for evading the LEP II constraint on M_{Higgs} without introducing severe fine-tuning. As discussed in [9], this happens if A_t is large, $\tan\beta$ is (moderately) large, and M_{mess} is small. In particular, it is crucial to have large A_t, compared with $m_{\tilde{t}}$, to evade the Higgs boson mass bound while keeping Δ^{-1} modest.

In Fig. 1, we plot minimal values of $m_{\tilde{t}} \equiv (m_{Q_3}^2)^{1/2} = (m_{U_3}^2)^{1/2}$, $m_{\tilde{t}}|_{\text{min}}$, that give $M_{\text{Higgs}} \gtrsim 114.4$ GeV as a function of $A_t/m_{\tilde{t}}$. The other parameters are fixed to be
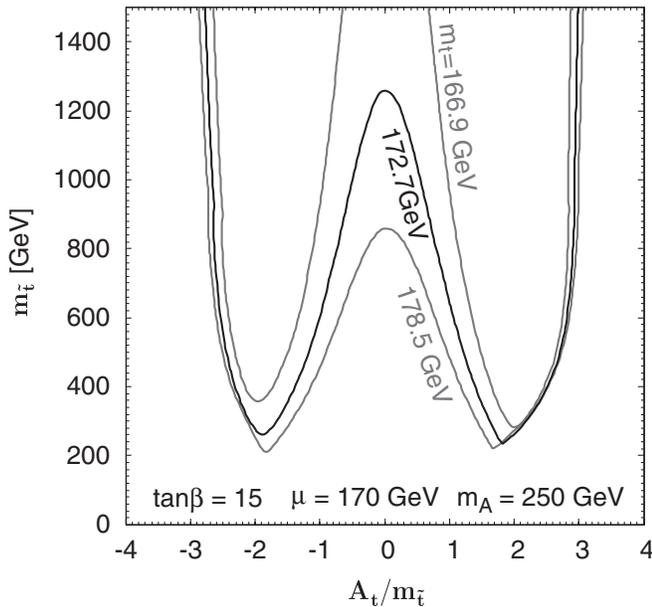
FIG. 1. Minimal values of $m_{\tilde{t}} \equiv (m_{Q_3}^2)^{1/2} = (m_{U_3}^2)^{1/2}$ giving $M_{\text{Higgs}} \gtrsim 114.4$ GeV as a function of $A_t/m_{\tilde{t}}$. The other parameters are fixed to be 500 GeV for the gaugino and sfermion masses other than $m_{Q_3}^2$ and $m_{U_3}^2$, $(500 \text{ GeV})(A_t/m_{\tilde{t}})$ for the A parameters other than A_t, $\tan\beta = 15$, $\mu = +170$ GeV, and $m_A = 250$ GeV.

500 GeV for the gaugino and sfermion masses other than $m_{Q_3}^2$ and $m_{U_3}^2$, $(500 \text{ GeV})(A_t/m_{\tilde{t}})$ for the A parameters other than A_t, $\tan\beta = 15$, $\mu = +170$ GeV, and $m_A = 250$ GeV, where m_A is the mass of the pseudoscalar Higgs boson. The dependence of the results on the fixed parameters is not significant, as long as $\tan\beta$ is sufficiently large, e.g., $\tan\beta \gtrsim 10$. In the figure we plot $m_{\tilde{t}}|_{\text{min}}$ for three different values of the top quark mass, $m_t = 166.9$, 172.7 and 178.5 GeV, corresponding to the central value and the 2σ range of the the latest experimental data: $m_t = 172.7 \pm 2.9$ GeV [25]. The calculation here has been performed using *FeynHiggs2.2* [26] (for earlier analyses for the Higgs boson mass in the MSSM, see e.g. [27]). If we instead use a code based on the pure $\overline{\text{DR}}$ scheme, such as `SuSpect 2.3` [28], we obtain slightly different values of $m_{\tilde{t}}|_{\text{min}}$: for $|A_t/m_{\tilde{t}}| \sim 2$ the differences are of order 50 GeV but for $|A_t/m_{\tilde{t}}| \ll 1$ the $\overline{\text{DR}}$ scheme calculation can give $m_{\tilde{t}}|_{\text{min}}$ larger than that in the figure by about 200 GeV. These differences give an estimate for the size of higher order corrections. Throughout the paper, our sign convention for μ and the soft supersymmetry-breaking parameters follows that of SUSY Les Houches Accord [29].

The figure clearly shows that in order to have light top squarks suggested by Eq. (6) the existence of a substantial A_t term ($|A_t/m_{\tilde{t}}| \gtrsim 1$) is required. For $m_t = 172.7$ GeV, the existence of A_t with $|A_t/m_{\tilde{t}}| \gtrsim 1$ can allow $m_{\tilde{t}}$ as small as $(200 \sim 400)$ GeV while $m_{\tilde{t}}$ should be larger than ≈ 1.2 TeV for $|A_t/m_{\tilde{t}}| \ll 1$. Another important point is that for $|A_t/m_{\tilde{t}}| \sim 2$, which gives the minimal value of $m_{\tilde{t}}|_{\text{min}}$, the sensitivity of $m_{\tilde{t}}|_{\text{min}}$ to the value of m_t is mild, while for $|A_t/m_{\tilde{t}}| \ll 1$ the sensitivity is huge. This implies, for example, that if m_t turns out to be smaller than $\simeq 170$ GeV theories with $|A_t/m_{\tilde{t}}| \ll 1$ at the weak scale will pretty much be "excluded."

We conclude that to have natural electroweak symmetry breaking in supersymmetric theories with the minimal, i.e. MSSM, matter content, the existence of a substantial A_t term at the weak scale is crucial. Another important ingredient is a moderately large $\tan\beta$, e.g. $\tan\beta \gtrsim 5$, to have a sufficiently large tree-level Higgs boson mass, which requires the holomorphic supersymmetry-breaking mass squared for the Higgs doublets, the μB term, to be (significantly) smaller than $2|\mu|^2 + m_{H_u}^2 + m_{H_d}^2$. In fact, these ingredients dominantly control the amount of fine-tuning in almost any theory with the MSSM matter content. To demonstrate this, we will now analyze the situations in the case of high scale supersymmetry-breaking and in gauge mediation models from the viewpoint of the size of A_t at the weak scale. For earlier analyses of fine-tuning in these models, see e.g. [30].

B. High scale supersymmetry breaking and gauge mediation

Let us first consider the minimal supergravity (mSUGRA) scenario [31]. We start by considering the
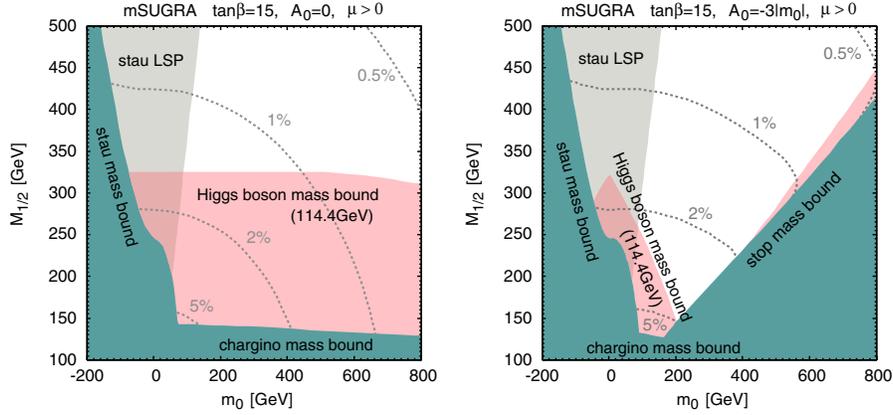
FIG. 2 (color online). Contours of Δ^{-1} on the $m_0 - M_{1/2}$ plane for the constrained mSUGRA with $A_0 = 0$ (left) and $A_0 = -3|m_0|$ (right). The sign of μ is chosen to be positive. The constraints from direct superparticle search, the Higgs boson mass bound, and the stau LSP are also shown.

constrained mSUGRA, in which the soft supersymmetry-breaking parameters are specified by the universal gaugino mass $M_{1/2}$, universal scalar mass squared m_0^2, universal A term A_0, and the μB term at the unification scale, $M_{\text{unif}} \approx 10^{16}$ GeV. While this scenario is sometimes criticized due to a lack of a strong theoretical motivation, it is not so bad in term of fine-tuning, compared with other models such as gauge mediation models. This is because we can obtain a reasonable size of $A_t/m_{\tilde{t}}$ at the weak scale, so that the top squark masses can be made smaller compared with the models giving smaller values of $A_t/m_{\tilde{t}}$ at the weak scale.

In Fig. 2 we plot values of the fine-tuning parameter Δ^{-1} in the constrained mSUGRA for two different choices of A_0: $A_0 = 0$ and $A_0 = -3|m_0|$. The parameter Δ^{-1} is defined by the fractional sensitivities of the electroweak VEV, $v \simeq 174$ GeV, to the fundamental parameters of the theory, with generic sensitivities of v to the parameters appropriately corrected [32]. We plot the contours of Δ^{-1} on the $m_0 - M_{1/2}$ plane for $\mu > 0$, where $m_0 \equiv \text{sgn}(m_0^2)|m_0^2|^{1/2}$. The values of μ and μB at M_{unif} are determined by v and $\tan\beta$, and we take $\tan\beta = 15$. We find that for $A_0 = 0$ the fine-tuning is worse than 2%, while for $A_0 = -3|m_0|$ it can be as mild as 5% for $M_{1/2} \simeq 150$ GeV and $m_0^2 \simeq (200 \text{ GeV})^2$. This can be understood as follows. For $A_0 = 0$, renormalization group equations give low-energy values for A_t and $m_{\tilde{t}}$ that satisfy $A_t/m_{\tilde{t}} \sim -1$. While this value of $|A_t/m_{\tilde{t}}|$ is not totally negligible, it is still not large enough to give $M_{\text{Higgs}} \gtrsim 114.4$ GeV with top squark masses smaller than about 600 GeV (see Fig. 1). This gives a high sensitivity of v to y_t (the top-stop contribution to $m_{H_u}^2$), leading to $\Delta^{-1} \lesssim 2\%$. The situation can be made better by introducing nonvanishing A_0 at M_{unif}. While the sensitivity of low-energy A_t to A_0 is rather weak, $A_0 = -3|m_0|$ can give a low-energy value of $A_t/m_{\tilde{t}}$ about -1.8, which allows $m_{\tilde{t}}$ as small as $\simeq 250$ GeV to evade the Higgs boson mass bound, and thus Δ^{-1} as large as 5%. Here $m_{\tilde{t}}$ is defined by $m_{\tilde{t}} \equiv (m_{Q_3}^2 m_{U_3}^2)^{1/4}$. In fact, larger values of A_0 do not help in reducing fine-tuning because of a shrinking

of the phenomenologically acceptable parameter region, and we obtain $\Delta^{-1}|_{\text{max}} \approx 5\%$ in the constrained mSUGRA.

In the case of the constrained mSUGRA described above, Δ^{-1} is determined by the sensitivity of v to y_t and μ, which implies that the dominant source of fine-tuning comes from the sensitivity of $m_{H_u}^2$ to the top-stop loop contribution. We can make this sensitivity weaker by deviating from the constrained mSUGRA. A simple way of doing this is to make $m_{H_u}^2$ and $m_{H_d}^2$ differ from m_0^2 at M_{unif}. Practically, this implies that we can take low-energy values of μ and m_A as free parameters. Then, for certain values of μ and m_A, which corresponds to choosing certain values of $m_{H_u}^2$ and $m_{H_d}^2$ at M_{unif}, we find that the sensitivity of v to y_t can be made weaker due to renormalization group properties of the soft supersymmetry-breaking parameters. This is illustrated in the left panel of Fig. 3, where we plot the contours of Δ^{-1} on the $m_0 - M_{1/2}$ plane, with $\mu = 190$ GeV, $m_A = 250$ GeV and $A_0 = -3|m_0|$. We find that fine-tuning can be made as mild as $\Delta^{-1} \simeq 8\%$. A similar reduction of tuning can also occur in the region with $m_{\tilde{t}}^2 < 0$ at M_{unif}, which is allowed if we violate the universality of $M_{1/2}$ and/or m_0^2 to avoid the slepton mass bound. This is illustrated in the right panel of Fig. 3 for $\mu > 0$, where we plot Δ^{-1} as a function of the gaugino mass, $M_{1/2}$, and the squark mass, $m_{\tilde{q}} \equiv \text{sgn}(m_{\tilde{q}}^2)|m_{\tilde{q}}^2|^{1/2}$, at the unification scale M_{unif}. The other parameters are chosen as $m_{\tilde{l}}^2 = (500 \text{ GeV})^2$ for the sleptons, $A_0 = -|m_{\tilde{q}}|$, and $m_{H_u}^2 = m_{H_d}^2 = (100 \text{ GeV})^2$ at M_{unif}. We find that fine-tuning can be as mild as $\Delta^{-1} \simeq 8\%$.[2]

---

[2]The region with $m_{\tilde{t}}^2 < 0$ has been discussed recently in [22] in the context of finding a relation among soft supersymmetry-breaking parameters which reduces fine-tuning. Our approach here is different: we do not assume any special relations among the supersymmetry-breaking masses, e.g., between the gaugino and squark masses. We then do not find a region with Δ^{-1} better than $\approx 10\%$.
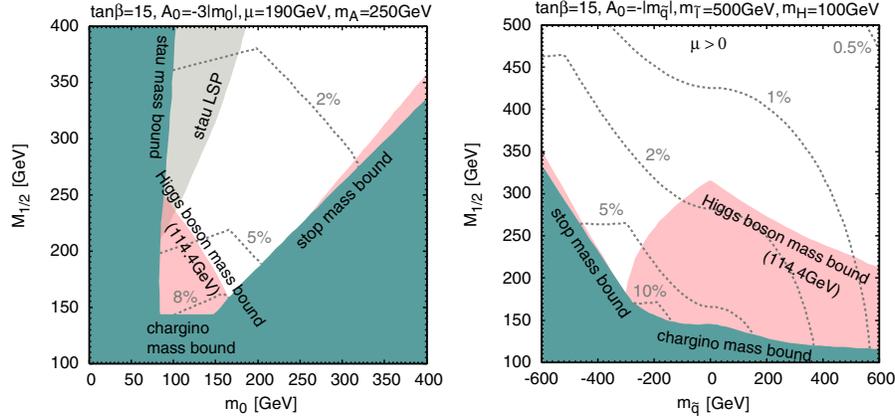
FIG. 3 (color online).   Contours of Δ^{-1} on the $m_0 - M_{1/2}$ plane in the mSUGRA model with $\mu = 190$ GeV and $m_A = 250$ GeV fixed at the weak scale and $A_0 = -3|m_0|$ at M_{unif} (left). Contours of Δ^{-1} on the $m_{\tilde{q}} - M_{1/2}$ plane with $\mu > 0$ and $m_{\tilde{l}}^2 = (500$ GeV$)^2$, $A_0 = -|m_{\tilde{q}}|$ and $m_H^2 \equiv m_{H_u}^2 = m_{H_d}^2 = (100$ GeV$)^2$ at M_{unif}, where $m_{\tilde{q}}^2$ and $m_{\tilde{l}}^2$ are the squark and slepton masses, respectively, (right). In both cases $\tan\beta = 15$.

How much can we reduce fine-tuning in a theory with high scale supersymmetry breaking? It is possible, after all, that the soft supersymmetry-breaking parameters are not calculable (easily) if they are generated through physics at the gravitational scale. Suppose, for example, that grand unification is realized in five dimensions and supersymmetry is broken on a brane on which the active gauge group is only $SU(3)_C \times SU(2)_L \times U(1)_Y$ [33]. Suppose also that all the gauge, matter and Higgs fields propagate in the bulk, so that they all feel supersymmetry breaking through the operators $[Z\mathcal{W}^\alpha \mathcal{W}_\alpha]_{\theta^2}$, $[(Z + Z^\dagger)\Phi^\dagger\Phi]_{\theta^4}$ and $[Z^\dagger Z\Phi^\dagger\Phi]_{\theta^4}$, where Z is the supersymmetry-breaking field, $\mathcal{W}_\alpha$ the gauge field-strength superfields, and Φ the matter and Higgs chiral superfields. (The μ and μB terms can also be generated through $[Z^\dagger H_u H_d + \mathrm{h.c.}]_{\theta^4}$ and $[Z^\dagger Z H_u H_d + \mathrm{h.c.}]_{\theta^4}$). Then, if there is a flavor symmetry in the bulk and on the supersymmetry-breaking brane, the generated supersymmetry-breaking masses can be flavor universal. The flavor symmetry is broken only on the other brane on which the Yukawa couplings are located. This setup leads to soft supersymmetry-breaking masses that are completely general other than the fact that they are flavor universal. In particular, there is no imprint on the superparticle masses from the underlying gauge unification.

It is, therefore, important to figure out the maximum value of Δ^{-1} one can obtain in generic high scale supersymmetry-breaking scenarios. We first note that there is a "model-independent" source of the sensitivity of v to the fundamental parameters—the sensitivity of v to the gluino mass, M_3, at M_{unif}. This is because M_3 always gives contributions that make $m_{\tilde{t}}$ grow at the infrared, which always pushes down the value of $m_{H_u}^2$ at the weak scale. Since the sign of the contributions is definite, we cannot weaken this sensitivity by complicating renormalization group evolutions for a fixed value of M_3. Now, there is a lower bound on M_3 at M_{unif} arising from the requirement

that a sufficiently large $A_t/m_{\tilde{t}}$ is obtained at the weak scale, without making A_t at M_{unif} extremely large and thus introducing a large sensitivity of v to A_t. We find $M_3(M_{\mathrm{mess}}) \gtrsim 150$ GeV, which leads to a factor of ≈ 10 stronger fractional variation of v when we vary M_3 at M_{unif}: $\partial \ln v/\partial \ln M_3 \approx 10$. We conclude that, without a special relation(s) among various soft supersymmetry-breaking parameters, the maximum value of Δ^{-1} in high scale supersymmetry breaking is

$$\Delta_{\max}^{-1}|_{M_{\mathrm{mess}} \sim M_{\mathrm{unif}}} \approx 10\%. \qquad (7)$$

This occurs in parameter regions in which $|A_t/m_{\tilde{t}}| \approx O(1.5 \sim 2.5)$, $|\mu| \lesssim 250$ GeV and $M_{\tilde{g}} \gtrsim 450$ GeV, where $M_{\tilde{g}}$ is the gluino mass at the weak scale. In particular, the best points in Fig. 3 both occur at $A_t/m_{\tilde{t}} \simeq -1.8$ and $m_{\tilde{t}} = (m_{Q_3}^2 m_{U_3}^2)^{1/4} \simeq 250$ GeV. The electroweak VEVs satisfy $\tan\beta \gtrsim 5$, and the Higgs boson mass is bounded by $M_{\mathrm{Higgs}} \lesssim 120$ GeV.

If we want to improve fine-tuning further, we must consider a theory that gives smaller values of M_{mess}, at least effectively, because an ultimate reason for the 10% tuning in Eq. (7) is the large logarithm $\ln(M_{\mathrm{mess}}/m_{\tilde{t}}) \simeq \ln(M_{\mathrm{unif}}/m_{\tilde{t}})$. An important class of theories giving small M_{mess} is gauge mediation models [34,35]. In these models, however, the size of A terms at M_{mess} is small, so that $|A_t/m_{\tilde{t}}| \lesssim 1$ at the weak scale. This requires large top squark masses to evade the Higgs boson mass bound, and thus leads to severe fine-tuning. In Fig. 4 we plot the contours of Δ^{-1} as a function of F/M_{mess} and M_{mess} for $\mu > 0$, in the minimal gauge mediation models with $n_{\mathrm{mess}} = 1$ and 4 pairs of messenger fields in the $\mathbf{5} + \mathbf{5}^*$ representation of $SU(5) \supset SU(3)_C \times SU(2)_L \times U(1)_Y$. Here, M_{mess} and F are the supersymmetric and
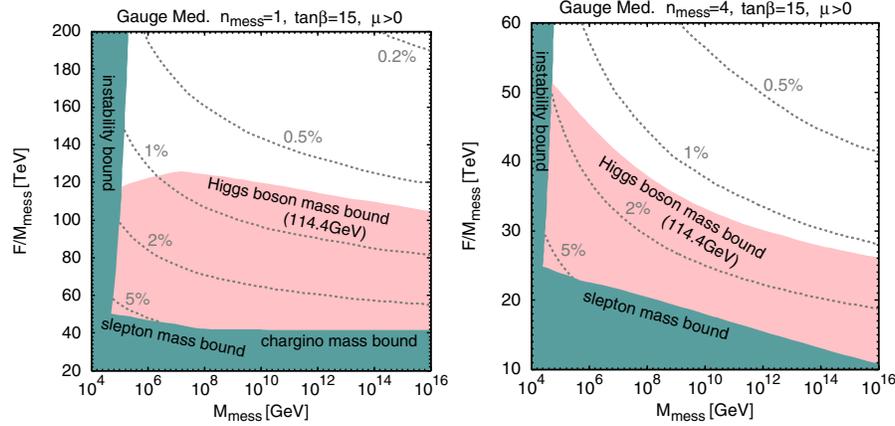
FIG. 4 (color online).   Contours of Δ^{-1} on the $M_{\text{mess}} - F/M_{\text{mess}}$ plane for the minimal gauge mediation models with $n_{\text{mess}} = 1$ (left) and $n_{\text{mess}} = 4$ (right) pairs of messenger fields in the $\mathbf{5} + \mathbf{5}^*$ representation. The instability bound implies the region in which the messenger fields are tachyonic, $F/|M_{\text{mess}}|^2 > 1$. The Higgs sector parameters are fixed as $\tan\beta = 15$ and $\mu > 0$.

supersymmetry-breaking masses for the messenger fields, respectively. We find that fine-tuning cannot be better than 2% over the entire parameter region.

C. Large A_t and small μB with low-scale M_{mess}

Discussions in the previous subsections show that the fine-tuning problem in minimal supersymmetry is solved if soft supersymmetry-breaking parameters are generated at a low scale with $|A_t|$ substantially (a factor of ~ 1.5 or so) larger than $m_{\tilde{t}}$. It is, however, not so easy to achieve this in a simple manner. Suppose, for example, that the superparticles obtain masses through direct couplings to the sector that dynamically breaks supersymmetry at a scale $\Lambda = O(10 \text{ TeV})$. This will generate both A terms and nonholomorphic supersymmetry-breaking squared masses, $\tilde{m}^2$, through operators of the form $[(Z + Z^{\dagger})\Phi^{\dagger}\Phi]_{\theta^4}$ and $[Z^{\dagger}Z\Phi^{\dagger}\Phi]_{\theta^4}$, where Z is the supersymmetry-breaking (composite) chiral superfield and Φ the quark, lepton and Higgs superfields. Flavor universality of the soft masses can be ensured by imposing a flavor symmetry on these couplings. Now, the strengths of these operators can be estimated using naive dimensional analysis [36]. We then find that the nonholomorphic masses are much larger than the A terms, $\tilde{m}^2 \approx (\Lambda/4\pi)^2$ and $A \approx \Lambda/16\pi^2$, leading to an unwanted result of $|A_t/m_{\tilde{t}}| \approx 1/4\pi \ll 1$. A possible way of avoiding this is to generate the operators given above in a perturbative regime at one and two loops, respectively, for example, by using messenger-matter mixing in gauge mediation. This leads to M_{mess} in the $O(10 \sim 100 \text{ TeV})$ region, allowing fine-tuning to be relaxed to the $(10 \sim 20)\%$ level with a modest logarithm of $\ln(M_{\text{mess}}/m_{\tilde{t}}) \simeq (3 \sim 6)$.

From the viewpoint of obtaining a large A term at low energies, the simplest possibility is to have the operators $[(Z + Z^{\dagger})\Phi^{\dagger}\Phi]_{\theta^4}$ (and $[Z^{\dagger}Z\Phi^{\dagger}\Phi]_{\theta^4}$) at tree level with $O(1)$ coefficients in units of the "cutoff" scale. Such a situation arises naturally if supersymmetry is broken asso-

ciated with an extra dimension(s) with the size of order $(10 \text{ TeV})^{-1}$ [37–41] and if matter and/or Higgs fields propagate in the extra dimension(s). Consider that the MSSM gauge, quark and lepton superfields propagate in an extra dimension compactified on S^1/Z_2 with the length πR. The two Higgs doublets are located on a brane, and the Yukawa couplings and the μ term are introduced there. Then, if the boundary conditions for these fields are twisted by the $SU(2)_R$ symmetry with an angle α, the theory just below $1/R$ is the MSSM with the soft supersymmetry-breaking parameters given by [40]

$$M_{1,2,3} = \frac{\alpha}{R}, \qquad m^2_{Q,U,D,L,E} = \left(\frac{\alpha}{R}\right)^2, \qquad A_{u,d,e} = -2\frac{\alpha}{R}, \tag{8}$$

$$m^2_{H_u,H_d} = 0, \qquad \mu B = 0, \tag{9}$$

where $M_{1,2,3}$ are the gaugino masses, and $m^2_{Q,U,D,L,E}$ and $A_{u,d,e}$ the flavor universal squark and slepton masses and A terms, respectively. Taking α/R to be a few hundred GeV and $1/R = O(10 \text{ TeV})$, this gives a perfect spectrum for electroweak symmetry breaking: the messenger scale is low, $M_{\text{mess}} \simeq 1/R$, $|A_t/m_{\tilde{t}}|$ is slightly smaller than 2 at the weak scale, and there is no strong hierarchy between the colored and noncolored superparticles. The origin of the small twist, $\alpha \approx (0.01 \sim 0.1)$, will lie in the dynamics of radius stabilization, as the $SU(2)_R$ twist in boundary conditions is equivalent to the supersymmetry-breaking VEV in the radion supermultiplet [42]. A trade-off of this theory is that we lose a conventional picture of the supersymmetric desert, and thus a simple understanding of successful supersymmetric gauge coupling unification [43], although it might arise, for example, through some conformal property above $1/R$ with the conformality vio-

lation effect associated somehow with the zero-mode representations.[3] In our view, the virtue of supersymmetric theories with a TeV extra dimension(s) lies in the fact that we can easily obtain large A terms at low scales. While the accommodation of the desert is nontrivial, we think that these theories provide a much more natural solution to the so-called little hierarchy problem [44] compared with any other nonsupersymmetric theories.

It is possible to obtain a picture similar to the one described above without losing the conventional supersymmetric desert. In a theory where the moduli [45] and anomaly mediated [46] contributions to supersymmetry breaking are comparable [47–50], the mediation scale of supersymmetry breaking, $M_{\rm mess}$, can be effectively lowered without having a real physical threshold at $M_{\rm mess}$ [48]. The soft supersymmetry-breaking parameters at $M_{\rm mess}$ are then given essentially by those of boundary condition supersymmetry breaking or (equivalently) moduli mediated supersymmetry breaking. (For a simple understanding of this property, see the Appendix.) One of the challenges to make a natural theory using this property is to have a sufficiently small μB term to obtain a sufficiently large $\tan\beta$. Because of a large gravitino mass required to employ anomaly mediation, it is rather difficult to achieve the desired level of a (very) small μB term.

A model having all the desired features to have natural electroweak symmetry breaking keeping the supersymmetric desert has been given in Refs. [9,10]. The effective messenger scale, $M_{\rm mess}$, is lowered to the TeV region, a large A_t term with $A_t/m_{\tilde t} \sim -1.4$ is obtained, and a large enough $\tan\beta$, $\tan\beta \gtrsim 5$, is accommodated by making μB small due to the renormalization group focusing effect and the elimination of the classical contribution. In the minimal setup, the soft supersymmetry-breaking parameters similar to those of Eqs. (8) and (9) are obtained at $M_{\rm mess} = O({\rm TeV})$:

$$M_{1,2,3} = M_0, \qquad m_{Q,U,D,L,E}^2 = \frac{M_0^2}{2}, \qquad A_{u,d,e} = -M_0,$$
(10)

$$m_{H_u,H_d}^2 = 0, \qquad \mu B = 0, \tag{11}$$

where M_0 is a parameter of order a few hundred GeV.[4]

---

[3]In such a scenario, the observed differences of the three low-energy gauge couplings should arise mainly from the differences of the gauge couplings in the bulk, and not from operators localized on a brane(s). Otherwise, the soft supersymmetry-breaking parameters in Eq. (8) would receive large corrections from brane operators, and the colored superparticles would become much heavier than the noncolored ones, leading to the pattern which is not desirable in terms of electroweak symmetry breaking.

[4]Note that the sign convention for the supersymmetry-breaking masses adopted here, i.e. that of Ref. [29], is different from those in Refs. [9–11]. In particular, the sign of the A terms is opposite.

Depending on the mechanism of μ and μB term generation, the parameter $B \equiv \mu B/\mu$ may have a nonzero value of order $M_0/4\pi$. As shown in Ref. [9], this theory does not suffer from fine-tuning, i.e. $\Delta^{-1} \gtrsim 20\%$, and the region giving $\Delta^{-1} \gtrsim 20\%$ is consistent with the experimental constraints, such as the one from $b \to s\gamma$, as long as the sign of μ is positive [11].[5] The essential point, again, is to generate a large $|A_t/m_{\tilde t}|$ and moderately large $\tan\beta$ with a small (effective) messenger scale, $M_{\rm mess} \sim {\rm TeV}$. Note that small effective $M_{\rm mess}$ is achieved here by having special relations among various supersymmetry-breaking parameters at $M_{\rm unif}$, which allows us to evade the general result of Eq. (7). The top squarks should be light to eliminate fine-tuning, although they do not have to be as light as in the case of high scale supersymmetry-breaking, because of rather small $M_{\rm mess}$. A detailed study of the LHC signatures in this particular model will be given in Sec. IV.

D. Characteristic spectra: light top squarks and light Higgsinos

Considerations so far have highlighted certain generic features for a superparticle spectrum that leads to natural electroweak symmetry breaking in minimal supersymmetric theories. These have been obtained by considering mainly the tension between the $m_{H_u}^2|_{\rm rad}$ term in Eq. (3) and the Higgs boson mass bound from LEP II. Another important constraint on the spectrum comes from the $|\mu|^2$ term in Eq. (3). The fine-tuning arising from this term is about $M_{\rm Higgs}^2/2|\mu|^2$, so that requiring $\Delta^{-1} \gtrsim 20\%$ (10%) leads to the bound $|\mu| \lesssim 190$ GeV (270 GeV). This implies that the Higgsinos should be much lighter than in typical mSUGRA or gauge mediation models, where relatively large top squark masses lead to a large μ parameter.

Taking all these together, we find that a supersymmetric theory that has the minimal matter content and reproduces naturally the correct scale for electroweak symmetry breaking should have the following properties for the superparticle spectrum:

(i) The A term for the top squarks is large, $|A_t/m_{\tilde t}| \approx (1.5 \sim 2.5)$ at the weak scale. This leads to a large mass splitting between the two top squarks:

$$m_{\tilde t_2} - m_{\tilde t_1} \approx (1.5 \sim 2.5)m_t. \tag{12}$$

Here, we have assumed $m_{Q_3}^2 \approx m_{U_3}^2$. The splitting as small as $\simeq m_t$, however, may be allowed if $M_{\rm mess}$ is small, $M_{\rm mess} = O({\rm TeV})$.

(ii) The top squarks should be light, i.e. $m_{\tilde t} \equiv (m_{Q_3}^2 m_{U_3}^2)^{1/4}$ should be small, to reduce the sensitivity of v to y_t. How small $m_{\tilde t}$ should be depends on the value of $M_{\rm mess}$ and the amount of Δ^{-1} required. For the case of high scale supersymmetry

---

[5]It is interesting to point out that the sign of μ is determined to be positive in the minimal setup, $\mu B = 0$ at $M_{\rm mess}$, as long as $M_{\rm mess}$ is larger than the weak scale.

breaking with $\Delta^{-1} \approx 10\%$, the bound is very strong, $m_{\tilde{t}} \lesssim 300$ GeV, leading to $m_{\tilde{t}_1} \sim 100$ GeV.

(iii) Small values for the top squark masses imply that we cannot push up the Higgs boson mass much larger than the tree-level value. Typically, we find

$$M_{\text{Higgs}} \lesssim 120 \text{ GeV}. \qquad (13)$$

(iv) The ratio of the electroweak VEVs should also be moderately large

$$\tan\beta \gtrsim 5, \qquad (14)$$

to have a sufficiently large Higgs boson mass at tree level. This implies that the μB term should be (significantly) smaller than $2|\mu|^2 + m_{H_u}^2 + m_{H_d}^2$ at the weak scale.

(v) The μ parameter should be small

$$|\mu| \lesssim 190 \text{ GeV}(270 \text{ GeV}), \qquad (15)$$

for $\Delta^{-1} \gtrsim 20\%$ (10%). This leads to light Higgsinos, which may be the LSP, or if not, may significantly mix with the LSP.

The features described above still leave several possible patterns for the superparticle spectrum, which can lead to somewhat different situations. In Fig. 5 we depict possible patterns which are representative for generic cases. In Fig. 5(a), we depict a pattern that typically arises in a high scale supersymmetry-breaking scenario with $\Delta^{-1} \approx 10\%$, for example, in the mSUGRA model with $m_{H_u}^2$, $m_{H_d}^2 \neq m_0^2$ (see Fig. 3). In this situation the top squarks are rather light, $m_{\tilde{t}} = (m_{Q_3}^2 m_{U_3}^2)^{1/4} \lesssim 300$ GeV, with the light top squark close to its experimental bound, $m_{\tilde{t}_1} \simeq 100$ GeV. The Higgsinos, $\tilde{h}$, are also light, although $\Delta^{-1} \approx 10\%$ allows $m_{\tilde{h}}$ as large as ≈ 270 GeV. In principle there are little constraints on the other gaugino and sfermion masses, except that the gluino should be heavier than about 450 GeV and that the squarks cannot be much

lighter than the gluino. The universal gaugino mass relation, $M_3/g_3^2 = M_2/g_2^2 = M_1/g_1^2$, may or may not be satisfied. The LSP will be either binolike, winolike, Higgsino-like, or a mixture of these states. If the LSP consists mainly of the bino, its thermal relic abundance can give the correct dark matter density either through a large mixture with the neutral Higgsinos and/or wino, coannihilation with the stau or stop, or resonant annihilation through s-channel Higgs boson exchange. Note that some of these options are not available in typical mSUGRA points, in which top squarks are heavy and thus the μ parameter is large. For other cases of winolike and Higgsino-like LSPs, the production should be nonthermal. It is interesting that a large A_t term also makes it easier to satisfy the constraints from the precision electroweak data with small top squark masses [51]. It is important to perform detailed LHC studies of this class of spectra, although a large ambiguity for the gaugino and sfermion masses will make a thorough study of the parameter space somewhat complicated. These spectra will also be interesting for a future e^+e^- linear collider [52].

If we want to reduce fine-tuning further, for example, to eliminate it altogether ($\Delta^{-1} \gtrsim 20\%$), we must generate the soft supersymmetry-breaking parameters at low energies. Because of a small logarithm, $\ln(M_{\text{mess}}/m_{\tilde{t}})$, constraints on the top squark sector is slightly weaker in this case: $|A_t/m_{\tilde{t}}| \gtrsim O(1)$ and $m_{\tilde{t}} \lesssim O(700 \text{ GeV})$. On the other hand, the constraint on the μ parameter is stronger because of a stronger requirement on Δ^{-1}: for $\Delta^{-1} \gtrsim 20\%$, we obtain the bound on the Higgsino masses $m_{\tilde{h}} \lesssim 190$ GeV. In fact, generating these spectra with small M_{mess} is nontrivial, and one of the ways is to adopt (effectively) the scheme of boundary condition, or moduli, supersymmetry breaking at low energies. This generically leads to a rather ordered spectrum at low energy, e.g. universal gaugino and sfermion masses at the weak scale. This situation is depicted in Fig. 5(b), where almost degenerate gaugino and sfermion masses are assumed. The relation between the gaugino and sfermion masses is model-dependent. An
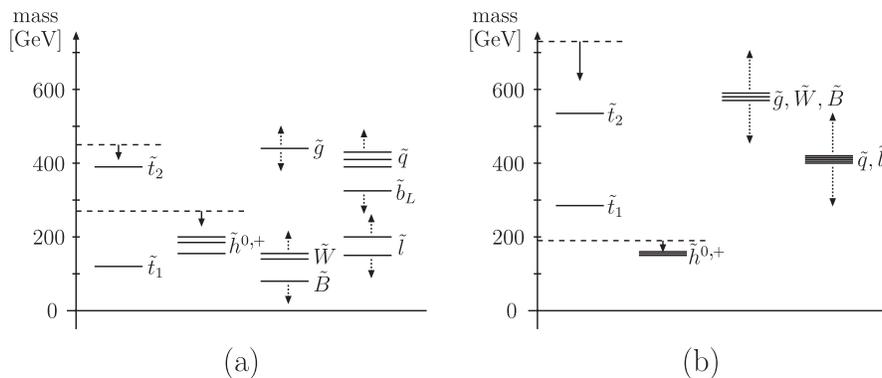
FIG. 5. Characteristic spectra for the superparticles which give the correct scale for electroweak symmetry breaking without significant fine-tuning. The spectrum in (a) arises typically in a high scale supersymmetry-breaking scenario with $\Delta^{-1} \approx 10\%$, while that in (b) arises in a theory where supersymmetry is broken by boundary conditions, or moduli contributions, with small (effective) M_{mess}.

important implication of this class of spectra is that the LSP is one of the neutral Higgsinos, unless the gravitino is lighter. To identify this LSP to be the dark matter, it must be produced nonthermally, for example, as in [53]. As discussed in [11], such dark matter can have an interesting implication on direct dark matter detection experiments such as CDMS II.

In the rest of the paper, we focus on studying LHC signatures for the latter class of spectra, given in Fig. 5(b). We do so partly because it gives milder (or no) fine-tuning, and partly because there is little LHC study directly related to this case. In particular, we first focus on signals expected from the Higgsino LSP at the LHC, and discuss under what conditions the signals are most useful. We then demonstrate in section IV that the signals can indeed be used in realistic analyses, using the explicit model discussed at the end of subsection II C. The determination of model parameters are also discussed there, which may be useful to discriminate between various possible models.

III. HIGGSINO LSP AT THE LHC

We have seen that in a large class of theories where the supersymmetric fine-tuning is solved, the Higgsinos are the lightest among the superpartners of the standard model particles. A characteristic pattern for the superparticle spectrum in these theories is depicted in Fig. 5(b). The three gauginos are almost degenerate at the weak scale, as well as the squarks and sleptons. The ratio of the gaugino and the sfermion masses is model-dependent. In this section, we identify characteristic signals of these spectra at the LHC, and discuss under what conditions the signals are useful in realistic analyses. We assume throughout that the gravitino is not lighter than the Higgsinos, so that the LSP is the lightest neutral Higgsino.[6]

A. Dilepton invariant mass distribution from $\tilde{\chi}_2^0 \to \tilde{\chi}_1^0 l^+ l^-$ in the Higgsino LSP scenario

An important feature of the spectra depicted in Fig. 5(b) is that there are three almost degenerate neutralino/chargino states, $\tilde{\chi}_1^0$, $\tilde{\chi}_2^0$ and $\tilde{\chi}_1^+$, with the masses $\approx |\mu| \lesssim 190$ GeV. If the gaugino masses are sufficiently larger than $|\mu|$, which we assume to be the case, these states are almost purely the Higgsinos, with the mass splittings given by

---

[6]In fact, none of our analyses changes unless the gravitino mass, $m_{3/2}$, is smaller than $O(1 \sim 10$ keV) because the lightest Higgsino then lives long enough so that it can be treated as a stable particle for collider purposes. For a smaller gravitino mass, the lightest Higgsino decays into a Higgs boson and a gravitino, followed by the Higgs boson decay $h \to b\bar{b}$. This can be used to measure the Higgs boson mass, e.g., by selecting four b-jet events and plotting $M_{b\bar{b}}$ invariant masses. For $m_{3/2} = O(0.01 \sim 1$ keV), we may also have displaced $b\bar{b}$ vertex signals.

$$m_{\tilde{\chi}_2^0} - m_{\tilde{\chi}_1^0} \simeq m_Z^2 \left(\frac{\cos^2\theta_W}{M_2} + \frac{\sin^2\theta_W}{M_1} \right), \quad (16)$$

$$m_{\tilde{\chi}_1^+} - m_{\tilde{\chi}_1^0} \simeq \frac{m_Z^2}{2} \left(\frac{\cos^2\theta_W}{M_2} + \frac{\sin^2\theta_W}{M_1} \right), \quad (17)$$

where we have assumed a moderately large $\tan\beta$, e.g. $\tan\beta \gtrsim 5$, θ_W is the Weinberg angle, and M_1 and M_2 are the $U(1)_Y$ and $SU(2)_L$ gaugino mass parameters, respectively. This implies that $\tilde{\chi}_2^0$ and $\tilde{\chi}_1^+$ undergo three-body decays to $\tilde{\chi}_1^0$. In particular, $\tilde{\chi}_2^0$ has the leptonic decay mode

$$\tilde{\chi}_2^0 \to \tilde{\chi}_1^0 l^+ l^-. \quad (18)$$

At hadron colliders, this decay mode can give important information on the properties of the initial- and final-state neutralinos [3,54–56]. Below we show that the dilepton arising from the decay of Eq. (18) can provide an important test for the Higgsino nature of the lightest two neutralinos $\tilde{\chi}_1^0$ and $\tilde{\chi}_2^0$.

The three-body decay $\tilde{\chi}_2^0 \to \tilde{\chi}_1^0 l^+ l^-$ occurs through the diagrams shown in Fig. 6. In the limit where the mass difference between the two neutralinos is much smaller than the Z boson mass and where the slepton masses are much larger than the decaying neutralino, $m_{\tilde{\chi}_2^0} - m_{\tilde{\chi}_1^0} \ll m_Z$ and $m_{\tilde{l}_L}, m_{\tilde{l}_R} \gg m_{\tilde{\chi}_2^0}$, the effects of these diagrams are described by a single low-energy $\tilde{\chi}_1^0 \tilde{\chi}_2^0 l^+ l^-$ four-Fermi operator for each chirality of leptons. This implies that the distribution shape of the dilepton invariant mass, $M_{ll} \equiv \sqrt{(p_{l^+} + p_{l^-})^2}$, is completely determined by the masses of the two neutralinos, $\tilde{\chi}_1^0$ and $\tilde{\chi}_2^0$, where p_{l^+} and p_{l^-} are the four-momenta of l^+ and l^-. Let us now adopt the phase convention in which all the mass eigenvalues and the mixing matrix elements for the neutralinos are taken to be real. This basis can always be taken as long as there is no CP violating effect in the neutralino mass matrix, which we assume throughout. We then obtain the following dilepton invariant mass distribution after performing appropriate phase space integrals:

$$\frac{d\Gamma(\tilde{\chi}_2^0 \to \tilde{\chi}_1^0 l^+ l^-)}{dM_{ll}}$$

$$\propto M_{ll} \sqrt{(m_{\tilde{\chi}_2^0}^2 - m_{\tilde{\chi}_1^0}^2)^2 - 2(m_{\tilde{\chi}_1^0}^2 + m_{\tilde{\chi}_2^0}^2)M_{ll}^2 + M_{ll}^4}$$

$$\times \{ (m_{\tilde{\chi}_2^0}^2 - m_{\tilde{\chi}_1^0}^2)^2 + (m_{\tilde{\chi}_1^0}^2 + m_{\tilde{\chi}_2^0}^2)M_{ll}^2 - 2M_{ll}^4$$

$$+ 6\eta_\chi m_{\tilde{\chi}_1^0} m_{\tilde{\chi}_2^0} M_{ll}^2 \}, \quad (19)$$

for $0 \le M_{ll} \le m_{\tilde{\chi}_2^0} - m_{\tilde{\chi}_1^0}$ and $d\Gamma(\tilde{\chi}_2^0 \to \tilde{\chi}_1^0 l^+ l^-)/dM_{ll} = 0$ for $M_{ll} > m_{\tilde{\chi}_2^0} - m_{\tilde{\chi}_1^0}$. Here, $m_{\tilde{\chi}_1^0} = |M_{\tilde{\chi}_1^0}|$ and $m_{\tilde{\chi}_2^0} = |M_{\tilde{\chi}_2^0}|$ are the absolute values for the two smallest neutralino mass eigenvalues $M_{\tilde{\chi}_1^0}$ and $M_{\tilde{\chi}_2^0}$ with $m_{\tilde{\chi}_1^0} < m_{\tilde{\chi}_2^0}$, and $\eta_\chi \equiv \text{sgn}(M_{\tilde{\chi}_1^0})\text{sgn}(M_{\tilde{\chi}_2^0})$ is the relative sign between them. In fact, with the LEP II bound on the Higgsino masses, the

FIG. 6. The diagrams contributing to the $\tilde{\chi}_2^0 \to \tilde{\chi}_1^0 l^+ l^-$ decay.

assumption of $m_{\tilde{\chi}_2^0} - m_{\tilde{\chi}_1^0} \ll m_Z$ implies that the two neutralinos are nearly degenerate: $\Delta m \equiv m_{\tilde{\chi}_2^0} - m_{\tilde{\chi}_1^0} \ll m_{\tilde{\chi}_1^0}$. The M_{ll} distribution is then further simplifies to

$$\frac{d\Gamma(\tilde{\chi}_2^0 \to \tilde{\chi}_1^0 l^+ l^-)}{dM_{ll}} \propto M_{ll} \sqrt{\Delta m^2 - M_{ll}^2}$$
$$\times \{2\Delta m^2 + (1 + 3\eta_\chi)M_{ll}^2\}, \quad (20)$$

for $0 \le M_{ll} \le \Delta m$ and $d\Gamma(\tilde{\chi}_2^0 \to \tilde{\chi}_1^0 l^+ l^-)/dM_{ll} = 0$ for $M_{ll} > \Delta m$.

There are two important features for the M_{ll} distribution in Eq. (20) which can be used to test the Higgsino LSP scenario. First, the endpoint of the distribution, $m_{\tilde{\chi}_2^0} - m_{\tilde{\chi}_1^0}$, is expected to be very small:

$$M_{ll}^{\max} = m_{\tilde{\chi}_2^0} - m_{\tilde{\chi}_1^0} \simeq \frac{m_Z^2}{M_0} = O(10 \text{ GeV}), \quad (21)$$

where we have set $M_0 \equiv M_1 \simeq M_2$. Given the LEP II bound on the chargino mass, such a small mass splitting between $\tilde{\chi}_1^0$ and $\tilde{\chi}_2^0$ cannot arise in a theory where the LSP is gauginolike and the three gauginos respect the universal mass relation, $M_3/g_3^2 = M_2/g_2^2 = M_1/g_1^2$. Second, the Higgsino LSP necessarily leads to the opposite signs between $M_{\tilde{\chi}_1^0}$ and $M_{\tilde{\chi}_2^0}$, so that $\eta_\chi = -1$ in Eqs. (19) and (20). This is because in the gauge eigenbasis the 2×2 neutral Higgsino mass matrix takes a purely off-diagonal form $((0, -\mu), (-\mu, 0))$, which gives one positive and one negative eigenvalues after diagonalization including the effects of mixing with the gaugino states. The resulting

distribution is quite different from the one with $\eta_\chi = +1$, which arises in the case of the gauginolike LSP with $\text{sgn}(M_1) = \text{sgn}(M_2)$.

In Fig. 7 we plot M_{ll} distributions calculated for several different choices for the soft supersymmetry-breaking parameters. In the left panel, we plot the M_{ll} distribution for the Higgsino LSP case by a solid curve. The curve is drawn using the complete expression with $\tan\beta = 10$, $M_1 = M_2 = 480$ GeV and $\mu = 170$ GeV, which gives $m_{\tilde{\chi}_2^0} - m_{\tilde{\chi}_1^0} \simeq 20$ GeV. We have varied the slepton masses $m_{\tilde{l}} \equiv m_{\tilde{l}_L} = m_{\tilde{l}_R}$ in the range $1.001 \le r_{\tilde{l}} \equiv m_{\tilde{l}}/m_{\tilde{\chi}_2^0} \le 10$, but it does not lead to any visible change of the curve. In the figure we have also drawn curves obtained using the approximate expression of Eq. (20) for $\eta_\chi = -1$ (dashed line) and $\eta_\chi = +1$ (dotted line). We find that the expression of Eq. (20) with $\eta_\chi = -1$ well approximates the full result. The small discrepancy arises from corrections higher order in $(\Delta m/m_Z)^2$. The right panel shows the M_{ll} distribution in the case of gauginolike $\tilde{\chi}_1^0$ and $\tilde{\chi}_2^0$ with $\text{sgn}(M_1) = \text{sgn}(M_2)$ (solid lines). The parameters are chosen to be $\tan\beta = 10$ and $\mu = 500$ GeV, and M_1 and M_2 are chosen such that the same values of $m_{\tilde{\chi}_1^0}$ and $m_{\tilde{\chi}_2^0}$ as in the left panel are obtained: $M_1 = 158$ GeV and $M_2 = 182$ GeV. The slepton masses are varied as $r_{\tilde{l}} \equiv m_{\tilde{l}}/m_{\tilde{\chi}_2^0} = 10, 1.1, 1.01, 1.001$ and we find that the M_{ll} distribution in this case depends on $m_{\tilde{l}}$ but only when it is very close to the $\tilde{\chi}_2^0$ mass. As in the left panel, we also draw curves obtained from Eq. (20) with $\eta_\chi = -1$ (dashed line)
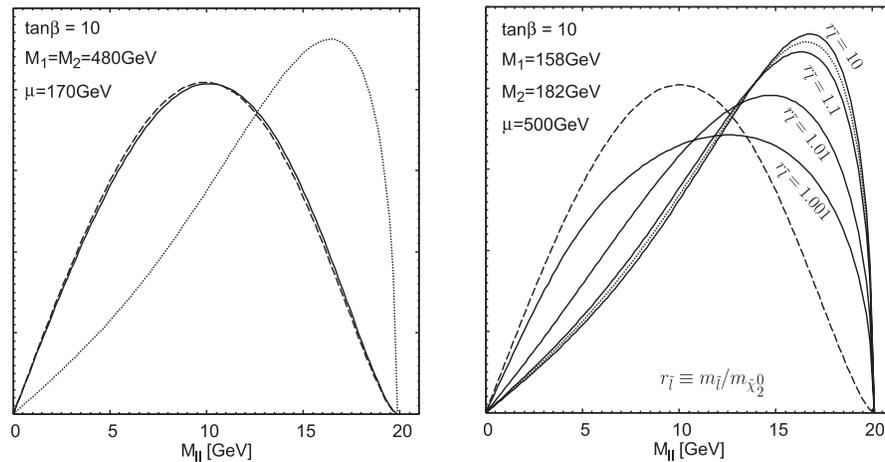
FIG. 7. Dilepton invariant mass distribution from the $\tilde{\chi}_2^0 \to \tilde{\chi}_1^0 l^+ l^-$ decay. Solid lines represent the distributions for the Higgsino LSP case (left panel) and the case of gauginolike $\tilde{\chi}_1^0$ and $\tilde{\chi}_2^0$ with $\text{sgn}(M_1) = \text{sgn}(M_2)$ (right panel). The curves with dashed and dotted lines represent the ones obtained from Eq. (20) with $\eta_\chi = -1$ and $+1$, respectively, (in both panels).

and $\eta_\chi = +1$ (dotted line). We find that the approximate curve with $\eta_\chi = +1$ well reproduces the full result with $r_{\tilde{l}} \gtrsim 1.1$.

The plots in Fig. 7 clearly show that the Higgsino LSP case can be discriminated from the case with $\eta_\chi \equiv \mathrm{sgn}(M_{\tilde{\chi}_1^0})\mathrm{sgn}(M_{\tilde{\chi}_2^0}) = +1$, even with the same mass difference $m_{\tilde{\chi}_2^0} - m_{\tilde{\chi}_1^0}$, regardless of the values for the other supersymmetry-breaking parameters such as the slepton masses. In particular, we find that the behavior of the M_{ll} distribution near the endpoint is completely different between the two cases of $\eta_\chi = -1$ and $+1$. This can be understood in terms of the selection rule for the orbital angular momentum due to the *CP* properties of the two neutralinos $\tilde{\chi}_1^0$ and $\tilde{\chi}_2^0$ [57]. For $\eta_\chi = +1$ (-1), the M_{ll} distribution near the kinematical endpoint, which corresponds to the limit of slow moving $\tilde{\chi}_1^0$ in the $\tilde{\chi}_2^0$ rest frame, should give an *S*-wave (*P*-wave) behavior, leading to $M_{ll} \propto (\Delta m - M_{ll})^{1/2}$ ($M_{ll} \propto (\Delta m - M_{ll})^{3/2}$) near the endpoint. While gauginolike $\tilde{\chi}_1^0$ and $\tilde{\chi}_2^0$ could potentially give a similar distribution if $\mathrm{sgn}(M_1) = -\mathrm{sgn}(M_2)$, the shape of the M_{ll} distribution together with the smallness of the endpoint can provide a powerful tool to test the Higgsino LSP scenario considered here, which necessarily leads to $\Delta m \ll m_Z$ and $\eta_\chi = -1$.[7]

To demonstrate that the signatures discussed above are really useful at the LHC, we must check that there are no other leptons from the superparticle cascade decays which bury the signatures. We must also show that the shape of the M_{ll} distribution from the $\tilde{\chi}_2^0 \rightarrow \tilde{\chi}_1^0 l^+ l^-$ decay is preserved under selection cuts in the analysis at a level that different shapes for $\eta_\chi = +1$ and -1 can be discriminated in a realistic detector. We address the first issue in the next subsection, in the context of a class of theories discussed in subsections II C and II D. The second issue will be addressed in Sec. IV, where we explicitly demonstrate that the M_{ll} distribution can indeed be used to test the Higgsino LSP scenario, as well as to extract the information on the neutralino masses, by performing Monte Carlo simulations using a specific theory.

B. Higgsino LSP with quasidegenerate gauginos and sfermions

Let us consider the pattern of the superparticle masses depicted in Fig. 5(b), which can naturally arise in a theory

where moduli-type, or boundary condition, supersymmetry breaking is employed with small M_{mess}. Specifically, we consider the following spectrum. The three gauginos are almost degenerate at the weak scale with the masses denoted by $m_{\tilde{g}}$. The squarks and sleptons are also nearly degenerate with the masses denoted by $m_{\tilde{q}}$, although the two top squarks, $\tilde{t}_1$ and $\tilde{t}_2$, can have substantially different masses because of a large mass splitting due to large A_t. The mass splittings among the gauginos and among different squarks and sleptons arise at higher order, but they are expected to be small and of $O(10\%)$. The μ parameter is smaller than about 200 GeV, so that it is smaller than both $m_{\tilde{g}}$ and $m_{\tilde{q}}$.

We first consider the case with $m_{\tilde{q}} < m_{\tilde{g}}$. In this case, a squark cannot decay into a gluino, so that it decays as $\tilde{q} \rightarrow \tilde{\chi}_1^+ q'$, $\tilde{\chi}_1^0 q$ or $\tilde{\chi}_2^0 q$. Here, q and q' represent quarks having the same and different flavors with $\tilde{q}$, and the lightest chargino, $\tilde{\chi}_1^+$, and the lightest two neutralinos, $\tilde{\chi}_{1,2}^0$, are the charged and neutral Higgsinos, respectively, with small mixings with the gaugino states. On the other hand, the gluino, once produced, decays into a quark and a squark $g \rightarrow q\tilde{q}$, followed by squark decay discussed above. In these decay chains, leptons arise only from decays of $\tilde{\chi}_1^+$ and $\tilde{\chi}_2^0$: $\tilde{\chi}_1^+ \rightarrow \tilde{\chi}_1^0 l^+ \nu$ and $\tilde{\chi}_2^0 \rightarrow \tilde{\chi}_1^0 l^+ l^-$. In the M_{ll} distribution analysis, we select events having two and only two leptons with the same flavor and opposite charge. The number of dileptons arising from $\tilde{\chi}_1^+$ decays is then small over the relevant energy region of $M_{ll} = O(10 \text{ GeV})$, compared with that from $\tilde{\chi}_2^0$ decay. (The background from $\tilde{\chi}_1^+$ decays can actually be estimated using opposite-sign opposite-flavor leptons and thus subtracted using the combination $e^+ e^- + \mu^+ \mu^- - e^+ \mu^- - \mu^+ e^-$.) The only remaining issue then is the squark branching ratio into $\tilde{\chi}_2^0$ and the $\tilde{\chi}_2^0$ branching ratio into leptons. In the parameter region we consider, the former is typically of $O(10\%)$ and the latter is $\approx 3\%$ for both $e^+ e^-$ and $\mu^+ \mu^-$ modes, which are large enough to produce an appreciable number of dilepton events.[8] We therefore conclude that the signatures discussed in the previous section can be used at the LHC for $m_{\tilde{q}} < m_{\tilde{g}}$. This claim will be confirmed in the next section, where we perform an explicit study using Monte Carlo simulations.

In the case of $m_{\tilde{q}} > m_{\tilde{g}}$, a squark decays mainly into a quark and a gluino, although it may also decay into a wino or bino by a small amount. The gluino then undergoes three-body decays: $\tilde{g} \rightarrow \tilde{\chi}_1^+ q\bar{q}'$, $\tilde{\chi}_1^0 q\bar{q}$ or $\tilde{\chi}_2^0 q\bar{q}$. The

---

[7]It is interesting to point out that the signatures discussed here arise only from the fact that the neutral Higgsinos are pseudo-Dirac fermions. The same technique, therefore, can also be used to test the idea of pseudo-Dirac gauginos, depending on the spectrum for the other superparticles (for examples of theories giving pseudo-Dirac gauginos, see [58]). For instance, if the LSP is one of the pseudo-Dirac bino or wino states, similar signatures may arise in the dilepton invariant mass distribution, depending on the existence of other sources of leptons and/or patterns of cascade decays for the superparticles.

[8]Strictly speaking, opposite-sign same-flavor dileptons may also arise from the three-body decay of the gluino $\tilde{g} \rightarrow \tilde{W}qq$ followed by the wino decay $\tilde{W} \rightarrow \tilde{l}l \rightarrow ll\tilde{\chi}_1^0$, if the gluino is slightly heavier than the wino, e.g. by about $O(10\%)$, due to higher order effects. The branching ratio of this mode, however, is extremely small because of a large phase space suppression, so that the resulting dileptons are completely negligible compared with the ones arising from $\tilde{\chi}_2^0$ decay. A similar comment also applies to $\tilde{q} \rightarrow ql\tilde{l}$ followed by $\tilde{l} \rightarrow l\tilde{\chi}_1^0$.

branching ratios for $\tilde{g} \to \tilde{W} q \bar{q}^{(\prime)}$, $\tilde{B} q \bar{q}$ may also be nonzero if the gluino is slightly heavier than the wino and/or bino, but these modes are highly suppressed by smallness of the phase space. The gluino branching ratio into $\tilde{\chi}_2^0$ is of $O(10\%)$, and the $\tilde{\chi}_2^0$ branching ratio into leptons (including both e and μ) is $\approx 6\%$, implying that an appreciable number of dilepton events can be obtained from $\tilde{\chi}_2^0$ decay. The background from $\tilde{\chi}_1^+$ decay is, again, not important. The only sources of leptons that could potentially destroy the signatures are decays of $\tilde{W}$ and $\tilde{B}$, produced by squark decay. The dominant decay modes of $\tilde{W}$ and $\tilde{B}$, however, will be into a Higgsino (either one of $\tilde{\chi}_1^+$, $\tilde{\chi}_1^0$ and $\tilde{\chi}_2^0$) and a W, Z or Higgs boson, so that the dangerous modes giving $l^+ l^-$ directly are suppressed by the three-body phase space and a small gaugino-Higgsino mixing. The number of dangerous dileptons from $\tilde{W}$ and $\tilde{B}$ decays, therefore, is at most of the same order as the ones from $\tilde{\chi}_2^0$ decay. Since the M_{ll} endpoint for these dileptons is about $m_{\tilde{g}} - |\mu|$ and the distribution is suppressed for M_{ll} much smaller than this values, it is unlikely that these leptons destroy the signatures from $\tilde{\chi}_2^0$ decay. (We select events having two and only two leptons when doing the M_{ll} analysis.) We thus find that the Higgsino LSP signatures discussed in the previous subsection are also useful in the case of $m_{\tilde{q}} > m_{\tilde{g}}$ at the LHC.

We finally consider the case where $m_{\tilde{q}} = m_{\tilde{g}}$ at the leading order (at tree level). In this case we expect that the masses of the gluino and squarks, $m_{\tilde{g}}$ and $m_{\tilde{q}}$, are slightly ($O(10\%)$) larger than those of the wino, bino and sleptons, $m_{\tilde{W}}$, $m_{\tilde{B}}$ and $m_{\tilde{l}}$, due to higher order (radiative) effects. The orderings among $m_{\tilde{g}}$ and $m_{\tilde{q}}$ and among $m_{\tilde{W}}$, $m_{\tilde{B}}$ and $m_{\tilde{l}}$ are model-dependent. With these spectra, gluinos and squarks once produced decay mostly into $\tilde{W}$ or $\tilde{B}$ plus a few jets, although a small fraction decays directly into light Higgsino states, $\tilde{\chi}_1^+$, $\tilde{\chi}_1^0$ and $\tilde{\chi}_2^0$. Decays of the electroweak gauginos differ depending on the ordering of $m_{\tilde{W}}$, $m_{\tilde{B}}$ and $m_{\tilde{l}}$. If there is a slepton with the mass smaller than that of a gaugino, e.g. $m_{\tilde{l}} < m_{\tilde{W}}$, there is a sizable branching ratio for the gaugino decaying into the slepton, $\tilde{W} \to l\tilde{l}$. This gives a large amount of opposite-sign same-flavor dileptons through the slepton decay $\tilde{l} \to l\tilde{\chi}_1^0$, which can potentially destroy the signatures from $\tilde{\chi}_2^0$ decay. On the other hand, if all the sleptons are heavier than $\tilde{W}$ and $\tilde{B}$, these gauginos decay mainly into a Higgsino (one of $\tilde{\chi}_1^+$, $\tilde{\chi}_1^0$ and $\tilde{\chi}_2^0$) and a W, Z or Higgs boson. The branching ratio into $\tilde{\chi}_2^0$ is typically of $O(10\%)$, and the desired signatures are obtained from $\tilde{\chi}_2^0$ decay. There are other dileptons from three-body decays of $\tilde{W}$ and $\tilde{B}$, such as $\tilde{W} \to \tilde{\chi}_1^+ ll$, but the number of these dileptons is sufficiently small. We thus expect that the Higgsino LSP signatures are useful for $m_{\tilde{q}} = m_{\tilde{g}}$ as long as all the sleptons are heavier than the electroweak gauginos.

We have seen that the Higgsino LSP signatures discussed in subsection III A are useful, i.e. not buried by dileptons from other superparticle decays, in a large class of theories motivated by solving the supersymmetric fine-tuning problem. In the next section, we explicitly demonstrate that these dilepton signatures can indeed be used in realistic analyses by performing Monte Carlo simulations in a theory with $m_{\tilde{g}} > m_{\tilde{q}}$. We also present a technique which can essentially determine all the superparticle masses in a class of theories discussed here, up to small mass splittings of $O(10\%)$ among different squarks and sleptons and a smaller splitting between the electroweak gaugino masses.

IV. NATURAL SUPERSYMMETRY AT THE LHC

In this section, we perform a Monte Carlo study for a class of theories discussed in the previous section and in subsections II C and II D which naturally leads to the correct scale for electroweak symmetry breaking. We explicitly demonstrate that the signatures discussed in the previous section can be used to test the Higgsino LSP and extract the small mass difference between the two neutral Higgsinos at the LHC. We also devise a series of cuts that allows us to determine all the relevant superparticle masses in theories with $m_{\tilde{g}} > m_{\tilde{q}}$: $m_{\tilde{\chi}_1^0}$, $m_{\tilde{q}}$, Δm and $m_{\tilde{g}}$. In particular, we perform the analysis in the context of the model based on mixed moduli and anomaly mediated supersymmetry breaking, discussed at the end of subsection II C, and show that the model can be tested at the LHC, up to theoretical uncertainties of $\approx 15\%$ on various superparticle masses.

A. Framework

The basic setup for our analysis is the same as that in subsection III B (and subsection II C). The three gauginos are almost degenerate at the weak scale, $m_{\tilde{g}} \equiv M_1 \simeq M_2 \simeq M_3$, and the squarks and sleptons are also nearly degenerate, $m_{\tilde{q}} \equiv (m_Q^2)^{1/2} \simeq (m_U^2)^{1/2} \simeq (m_D^2)^{1/2} \simeq (m_L^2)^{1/2} \simeq (m_E^2)^{1/2}$. The A parameters are nearly universal at the weak scale, $A \equiv A_u \simeq A_d \simeq A_e$, with A satisfying $|A/m_{\tilde{q}}| \gtrsim O(1)$. The (top) squark masses, $m_{\tilde{q}}$, should not be very large, and the ratio of the electroweak VEVs should satisfy $\tan\beta \gtrsim 5$. In the analysis in this section, we only consider the case $m_{\tilde{g}} > m_{\tilde{q}}$.

To perform an explicit Monte Carlo study, we must choose particular parameter points. For this purpose, we take the model based on mixed moduli and anomaly mediated supersymmetry breaking, discussed at the end of subsection II C, and choose the parameters within the region satisfying the condition $\Delta^{-1} \gtrsim 20\%$. In particular, we take [9,10]

$$M_{1,2,3} = M_0, \qquad m_{Q,U,D,L,E}^2 = \frac{M_0^2}{2},$$

$$A_{u,d,e} = -M_0, \qquad m_{H_u,H_d}^2 = O\left(\frac{M_0^2}{8\pi^2}\right), \tag{22}$$

at some scale $M_{\text{mess}} = O(100 \text{ GeV} \sim \text{TeV})$, where

$$450 \text{ GeV} \lesssim M_0 \lesssim 900 \text{ GeV}, \tag{23}$$

for $\tan\beta \gtrsim 20$. For smaller $\tan\beta$, the lower bound in Eq. (23) increases; for $\tan\beta = 10$ (5) the lower bound becomes $\approx 550 \text{ GeV}$ (900 GeV). In our analysis, we take μ, m_A and $\tan\beta$ to be free parameters in the Higgs sector, which are left undetermined after the electroweak symmetry breaking condition is imposed on μ, μB, $m_{H_u}^2$ and $m_{H_d}^2$. As shown in Ref. [11] the constraint from the $b \to s\gamma$ decay chooses the sign of μ to be positive. We thus have

$$\text{sgn}(\mu) = +1, \qquad |\mu| \lesssim 190 \text{ GeV},$$
$$m_A \lesssim 300 \text{ GeV}, \qquad \tan\beta \gtrsim 5. \tag{24}$$

The last three conditions come from the naturalness criterion, $\Delta^{-1} \geq 20\%$.

In our Monte Carlo study, we choose two parameter points given in Table I, satisfying Eqs. (22)–(24). The point I is representative for the case with a relatively low superparticle mass scale, while the point II for the case with a high superparticle mass scale. These points satisfy the experimental constraints such as the ones coming from the Higgs boson mass and the $b \to s\gamma$ decay, within theoretical uncertainties. We note, however, that the constraints from the Higgs boson mass and $b \to s\gamma$ are not very important in our present context, because they are sensitive to the parameters in the Higgs sector, such as m_A and $\tan\beta$, whose precise values are not relevant in our LHC study below.

The physical masses for the superparticles are obtained from the inputs in Table I as follows. We interpret the input masses as the running masses in the $\overline{\text{DR}}'$ scheme at the scale M_{mess}, and evolve them down to the superparticle mass scale using renormalization group equations. We then add the effects of electroweak symmetry breaking, such as the D-term contributions to the scalar masses and the gaugino-Higgsino mixings, and convert the running masses to the pole masses by including finite threshold corrections, using the code `SuSpect 2.3` [28]. The resulting superparticle masses are given in Table II for the two parameter points in Table I. Strictly speaking, this procedure is not quite meaningful in the context of the model under study, because we generically expect unknown

higher order corrections of $O(1/8\pi^2)$ in the expression of Eq. (22), which can be comparable to some of the low-energy corrections included here. Nevertheless, this procedure allows us to incorporate the fact that the colored particles are systematically heavier than the noncolored ones by $O(10\%)$, which we expect to hold in realistic situations. We thus perform our Monte Carlo study using the masses given in Table II, although one should remember that there are intrinsic theoretical uncertainties of $O(10\%)$ for the superparticle masses in the model.

To perform the analysis, we generate both supersymmetric and standard model events using `PYTHIA 6.324` [59]. We generate supersymmetric events for the two parameter points in Table I. The number of events generated for each point is equivalent to the integrated luminosity of 30 fb^{-1}, which corresponds to the three-year running of the LHC at low luminosity. The superparticle decays are calculated using the code `SDECAY 1.1a` [60], with the results transferred to `PYTHIA` and used in the event generation. For the estimation of standard model background, we have generated 0.5M QCD $2 \to 2$ events for each bin of the transverse momentum: $100 \text{ GeV} < p_T < 200 \text{ GeV}$, $200 \text{ GeV} < p_T < 400 \text{ GeV}$, $400 \text{ GeV} < p_T < 800 \text{ GeV}$, and $p_T > 800 \text{ GeV}$. We have also generated the $W + \text{jets}$ events with $W \to e\nu$, $\mu\nu$, $\tau\nu$ (0.5M events for $50 \text{ GeV} < p_T < 200 \text{ GeV}$ and 0.2M events for $p_T > 200 \text{ GeV}$), the $Z + \text{jets}$ events with $Z \to \nu\bar{\nu}$, $\tau^+\tau^-$ (0.5M events for

TABLE II. Superparticle masses in GeV for points I and II in Table I. The masses for the second generation squarks and sleptons are not listed because they are nearly degenerate with the corresponding first generation squarks and sleptons.

	point I	point II
$\tilde{g}$	623	917
$\tilde{\chi}_1^+$	167	170
$\tilde{\chi}_2^+$	600	893
$\tilde{\chi}_1^0$	161	166
$\tilde{\chi}_2^0$	177	176
$\tilde{\chi}_3^0$	584	882
$\tilde{\chi}_4^0$	603	894
$\tilde{u}_L$	473	686
$\tilde{u}_R$	471	684
$\tilde{d}_L$	480	691
$\tilde{d}_R$	472	685
$\tilde{e}_L$	433	643
$\tilde{e}_R$	429	640
$\tilde{\nu}_{eL}$	425	638
$\tilde{t}_1$	365	571
$\tilde{t}_2$	576	783
$\tilde{b}_1$	463	678
$\tilde{b}_2$	481	691
$\tilde{\tau}_1$	424	636
$\tilde{\tau}_2$	437	646
$\tilde{\nu}_{\tau L}$	425	638

TABLE I. Two representative parameter points of the model used in Monte Carlo simulations.

	point I	point II
M_0 [GeV]	600	900
μ [GeV]	170	170
m_A [GeV]	250	250
$\tan\beta$	15	15
M_{mess}	1 TeV	1 TeV

50 GeV $< p_T <$ 150 GeV and 0.2M events for $p_T >$ 150 GeV), 1M events for the $t\bar{t}$ production, and 0.2M events for each ZZ, $Z\gamma^*$, ZW and WW production. These standard model events are simply scaled to 30 fb^{-1} when estimating standard model backgrounds. While our background estimations are correct probably only to a factor of a few due to inherent uncertainties associated with the QCD effects, we expect that our analysis is not much affected by this because the standard model background can be pretty much reduced by our cut selections, as we will see later. Some of the analysis, e.g. the effective mass analysis in subsections IV D and IV E, may be affected by these uncertainties, but then we can always raise the cut on E_T^{miss} and recover the usefulness of the analysis.

For the detector simulation, we use `AcerDET 1.0` [61], a generic fast detector simulation and reconstruction package for the LHC, which has a similar principle of operation to the official fast simulation package of the ATLAS detector, `ATLFAST` [62]. The package performs identification and isolation of leptons, photons and jets in terms of detector coordinates: pseudorapidity η, azimuthal angle ϕ, and cone size $\Delta R = \sqrt{(\Delta\phi)^2 + (\Delta\eta)^2}$. Lepton, photon and jet four-momenta are smeared, and the cluster selections are made based on p_T and $|\eta|$. Isolation criteria are applied to leptons and photons in terms of the distance from other clusters, $\Delta R > 0.4$, and of maximum transverse energy deposited in cells in a cone $\Delta R = 0.2$ around the cluster. The calibration of jet four-momenta is also performed, and each jet is labeled either as a light jet, b-jet, c-jet or τ-jet, using information from event generators. (We use default parameters for these selection, isolation, calibration and labeling processes.) For the b-jet identification, we further implement b-tagging efficiency of 60% per a b-labeled jet, with mistagging probability of 10% for a c-labeled jet and 1% for a light jet. For the τ-jets, we use efficiency of 50% per a τ-labeled jet, with the mistagging probability of 10% for other jets.

For each event, we apply the following trigger selections [62]: one isolated electron with $p_T > 20$ GeV, one isolated photon with $p_T > 40$ GeV, two isolated electrons/photons with $p_T > 15$ GeV, one muon with $p_T > 20$ GeV, two muons with $p_T > 6$ GeV, one isolated electron with $p_T > 15$ GeV and one isolated muon with $p_T > 6$ GeV, one jet

with $p_T > 180$ GeV, three jets with $p_T > 75$ GeV, and four jets with $p_T > 55$ GeV, where isolated electrons/photons, isolated muons and jets must be in the central regions of pseudorapidity $|\eta| < 2.5$, 2.4, and 3.2, respectively. In our analysis, we consider only events passing one of these criteria.

In our study, we ignore possible systematic errors caused by cuts and choices of fitting functions and regions, and take only into account the statistical errors. Based on good agreements between the input values and the fit results obtained in subsections IV C, IV D, and IV E, however, we expect that these neglected errors are not much larger than the statistical errors included in the analysis. We also do not include detector issues such as fake leptons, but we expect, based on rough estimates, that they do not eliminate our signatures. Detailed studies of these issues, however, are warranted.

B. Characteristic features: short cascades and fewer leptons

We begin by identifying characteristic features relevant to the LHC arising for the superparticle spectra under consideration. At the LHC, most of the superparticle productions comes for $m_{\tilde{q}}$, $m_{\tilde{g}} \lesssim 1$ TeV from squark and gluino productions. For point I (point II) in Table I, the cross sections are $\simeq 3.8$ pb, 25.3 pb and 23.0 pb (0.27 pb, 2.98 pb and 3.71 pb) for the $\tilde{g}\tilde{g}$, $\tilde{g}\tilde{q}$ and $\tilde{q}\tilde{q}$ productions, respectively, where the total superparticle production cross section is about 55.2 pb (9.22 pb). We find that the squark-gluino pair production and the squark pair production dominate in our parameter space. After the production, a squark decays mostly into $\tilde{\chi}_1^+$ or $\tilde{\chi}_1^0$ and a quark, $\tilde{q} \rightarrow \tilde{\chi}_1^+ q'$, $\tilde{\chi}_1^0 q$, but it also decays into $\tilde{\chi}_2^0$, $\tilde{q} \rightarrow \tilde{\chi}_2^0 q$, with a small branching ratio of $O(10\%)$. The $\tilde{\chi}_1^+$ and $\tilde{\chi}_2^0$ produced then decay into $\tilde{\chi}_1^0$ and quarks/leptons through three-body decays, giving leptons with branching fractions of $O(10\%)$. For the gluino, it decays into a quark and a squark with the branching ratio of $\approx 100\%$, which is followed by squark decay.

An important feature of these decays is that the decay chains are relatively short. Compared with the case where the wino decay into a slepton is open, for example, decay chains with the present spectra are shorter in average.
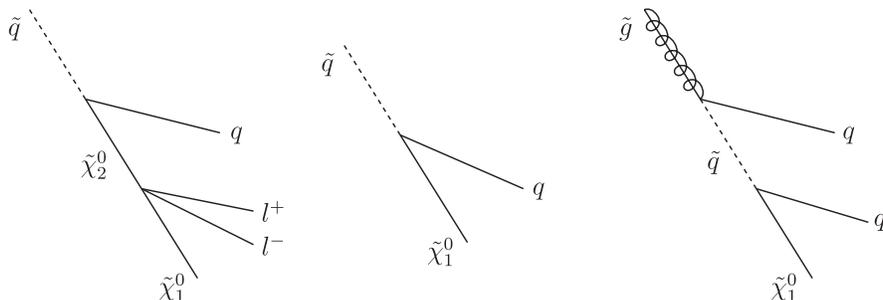
FIG. 8.   Decay cascades used in the analysis.

Another important feature is that the number of leptons arising in the cascades is significantly smaller than in the case where colored and noncolored superparticles have a large mass hierarchy, e.g. as in a typical mSUGRA parameter point. We can thus use (# of 1 lepton events)/(# of 0 lepton events) to make a first guess that the superparticles may have a spectrum like the one considered here. In fact, the features described here allow us to test certain generic aspects of the spectra, such as the nature of the LSP, and to determine the basic mass parameters in a simple manner. These information can then be used to test or discriminate between possible models, as will be discussed in subsection IV F.

In our analysis, the following decay cascades are used: $\tilde{q} \to \tilde{\chi}_2^0 q \to \tilde{\chi}_1^0 l^+ l^- q$, $\tilde{q} \to \tilde{\chi}_1^0 q$, and $\tilde{g} \to \tilde{q} q \to \tilde{\chi}_1^0 q q$, which are depicted in Fig. 8. Here, we have not discriminated between quarks and antiquarks. Using the kinematics of these cascades, we can determine the masses of the gluino, squarks and neutralinos, as well as the small mass difference between $\tilde{\chi}_1^0$ and $\tilde{\chi}_2^0$, model independently. This will be shown in subsections IV C and IV D for the case of point I and in subsection IV E for the case of point II. Various kinematical endpoints, such as the ones for dileptons, two leptons plus a jet, and a combination of two jets, will be used. Precisions of order a few to 10% are achieved, as will be shown later below.

C. Determination of the squark and neutral Higgsino masses

In this subsection we show that using the kinematics of the cascade decay $\tilde{q} \to \tilde{\chi}_2^0 q \to \tilde{\chi}_1^0 l^+ l^- q$ and those for the squark pair production with $\tilde{q} \to \tilde{\chi}_1^0 q$, we can determine $m_{\tilde{q}}$, $m_{\tilde{\chi}_1^0}$ and $m_{\tilde{\chi}_2^0}$ without using input from particular models. This information can thus be used for nontrivial tests of the model predictions, as will be discussed in subsection IV F. The analysis also demonstrates that the M_{ll} distribution discussed in Sec. III is indeed useful in testing the Higgsino nature of the lightest neutralinos. In this and the next subsections, we use point I in Table I ($M_0 = 600$ GeV) for the analysis. The same analysis will be repeated for point II ($M_0 = 900$ GeV) in subsection IV E.

We first look at the M_{ll} distribution from the three-body decay $\tilde{\chi}_2^0 \to \tilde{\chi}_1^0 l^+ l^-$. As discussed in Sec. III the endpoint and the shape of the distribution measure the mass difference of the two neutralinos, Δm, as well as the relative CP property of the two neutralinos, η_χ.

We select the dilepton events with the following cuts:
  (i) $E_T^{miss} > 300$ GeV
  (ii) At least two jets with $p_T > 50$ GeV
  (iii) Two and only two leptons with the same flavor and opposite charge
  (iv) Veto b-jets
In Fig. 9, we show the M_{ll} distribution obtained with the cuts described above. The standard model backgrounds are
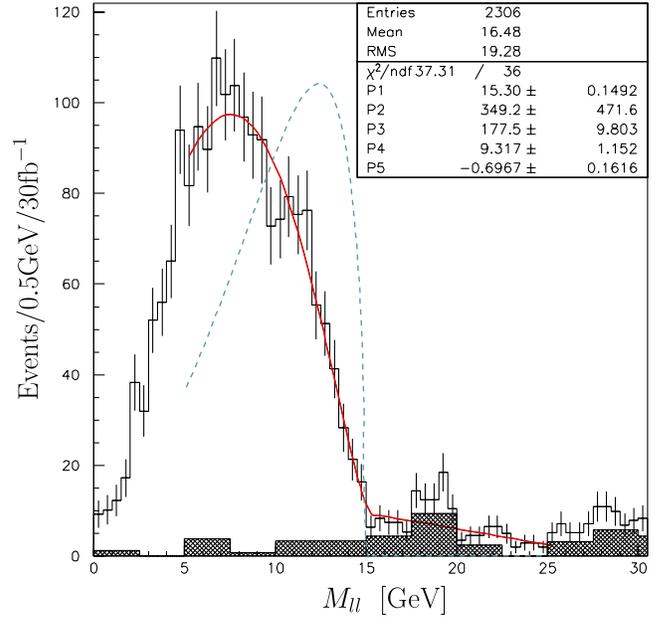
FIG. 9 (color online).   The distribution of the dilepton invariant mass, M_{ll}, for point I. Hatched histogram represents the standard model background, which is smeared over five bins in order not to magnify the statistical uncertainty due to the scaling of the events. The solid line is the best fit function for the signal plus background, obtained using the theoretical curve with $\eta_\chi = -1$. It can be clearly distinguished from the $\eta_\chi = +1$ case, drawn by the dashed line. The endpoint is extracted to be 15.30 ± 0.15 GeV.

effectively reduced by the cuts (hatched histogram). We can clearly see the endpoint of M_{ll} around 15 GeV, which can be the first test for the Higgsino LSP scenario. Note that while M_{ll} is small, p_T's of the leptons are not so small because of the parent $\tilde{\chi}_2^0$'s transverse momenta, so that these leptons are not much affected by the trigger selections of subsection IV A.

We have performed a fit of the distribution by using the theoretical curve including the effect of the finite Z-boson mass, with a linear background distribution. In this fitting process, the standard model background events are smeared in order not to artificially magnify the statistical uncertainty due to the scaling of the generated events to 30 fb^{-1}. A reasonable fit is possible only for the $\eta_\chi = -1$ case (solid line), and we obtain the endpoint value

$$M_{ll}^{max} = 15.30 \pm 0.15 \text{ GeV}, \tag{25}$$

which is consistent with the input value of the mass difference $\Delta m = 15.40$ GeV (see Eq. (21)). The theoretical curve with the $\eta_\chi = +1$ case is superimposed in the plot (dashed line). We can clearly see the deviation from the simulated distribution, especially near the endpoint. We thus conclude that the smallness of the endpoint, M_{ll}^{max}, together with the shape of the M_{ll} distribution characteristic of $\eta_\chi = -1$, provide an extremely powerful test for the Higgsino LSP scenario. If these signals are actually

observed, they strongly suggest that the LSP is one of the nearly degenerate neutral Higgsinos.

At this stage, we only have information on the neutralino mass difference, but further information can be obtained by stepping up the cascade, i.e. by combining dileptons with the quark jet from the squark decay. We can construct two independent Lorentz-invariant quantities M_{llq} and M_{lq}, whose endpoint values are given by

$$M_{llq}^{max} = M_{lq}^{max} = m_{\tilde{q}}\left(1 - \frac{m_{\tilde{\chi}_2^0}^2}{m_{\tilde{q}}^2}\right)^{1/2}\left(1 - \frac{m_{\tilde{\chi}_1^0}^2}{m_{\tilde{\chi}_2^0}^2}\right)^{1/2}. \quad (26)$$

The two endpoints coincide because the final-state leptons come from the three-body decay. The measurement of the two endpoints, therefore, can give only one additional information.

For the event selection for the M_{llq} and M_{lq} measurements, we have imposed a cut on M_{ll}

(i) $M_{ll} < 15$ GeV

in addition to the cuts for the M_{ll} measurement, in order to reject incorrect lepton pairs. The jet which is combined with the lepton(s) is selected from the two largest p_T jets. We choose the one that gives the smaller M_{llq} to see the endpoint of the distribution.

In Fig. 10, we show the distributions of M_{llq} (left) and M_{lq} (right). The endpoint is clearer in M_{llq} than in M_{lq}. We thus use the M_{llq} endpoint for the mass determination. We have performed a fit of the M_{llq} distribution near the endpoint, with a linear function with Gaussian smearing. A linear function is also assumed for the background distribution. The best fit function is drawn in the figure, and we obtain

$$M_{llq}^{max} = 179.6 \pm 5.8 \text{ GeV}. \quad (27)$$

This is consistent with the expected endpoint obtained using the formula of Eq. (26), which is $\simeq 180$ GeV. We have also tried to estimate the endpoint in the M_{lq} distribution. A reasonable fit, however, cannot be obtained with linear functions. Better functions are needed if one wants to extract the endpoint from the M_{lq} distribution. From the M_{ll} and M_{llq} endpoint measurements, we now have two relations among three mass parameters, $m_{\tilde{\chi}_1^0}$, $m_{\tilde{\chi}_2^0}$ and $m_{\tilde{q}}$. We still need one more independent quantity to determine all the three masses.

In principle, the threshold value of M_{llq} with the cut $M_{ll} > \xi M_{ll}^{max}$ ($0 < \xi < 1$) could provide the required additional information:

$$M_{llq}^{min}\big|_{M_{ll}>\xi M_{ll}^{max}} = \frac{M_{llq}^{max}}{\sqrt{2}}\left[1 - \frac{((1 + \xi^2 + (1 - \xi^2)\frac{m_{\tilde{\chi}_1^0}}{m_{\tilde{\chi}_2^0}})^2 - 4\xi^2)^{1/2}}{1 + \frac{m_{\tilde{\chi}_1^0}}{m_{\tilde{\chi}_2^0}}} + \xi^2\frac{1 + \frac{m_{\tilde{\chi}_2^0}^2}{m_{\tilde{q}}^2}}{1 - \frac{m_{\tilde{\chi}_2^0}^2}{m_{\tilde{q}}^2}}\frac{1 - \frac{m_{\tilde{\chi}_1^0}}{m_{\tilde{\chi}_2^0}}}{1 + \frac{m_{\tilde{\chi}_1^0}}{m_{\tilde{\chi}_2^0}}}\right]^{1/2}. \quad (28)$$
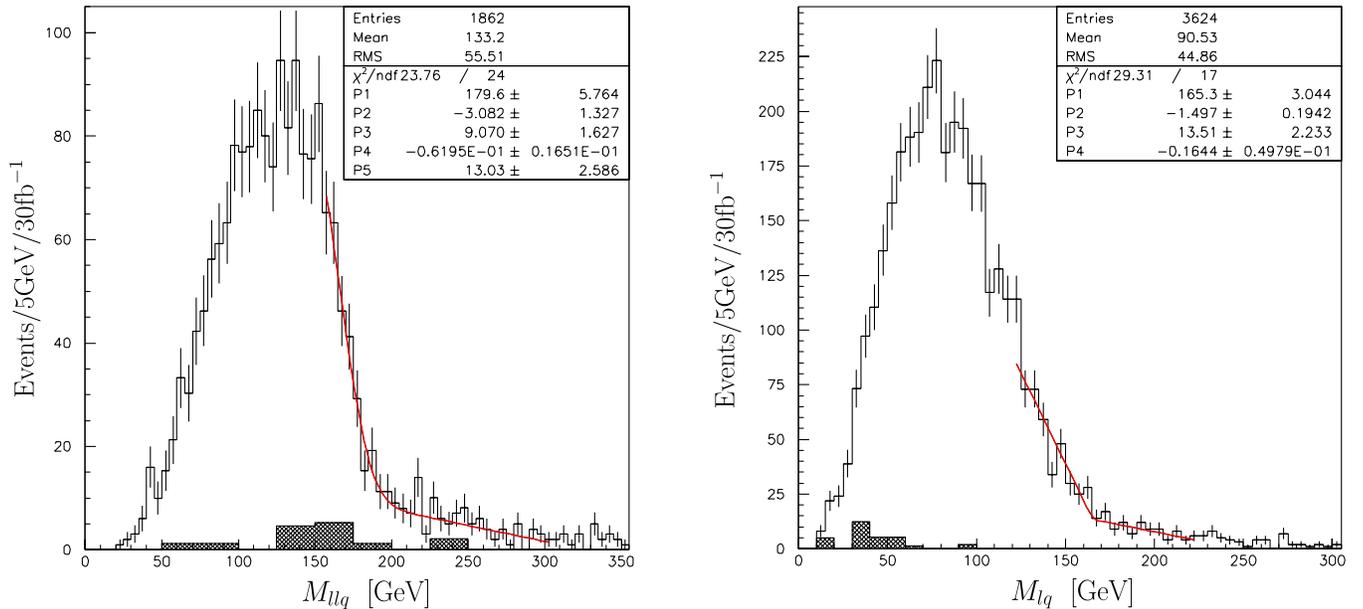
FIG. 10 (color online). The distributions of M_{llq} (left) and M_{lq} (right) for point I. Hatched histogram represents the standard model background, which for M_{llq} is smeared over five bins in order not to magnify the statistical uncertainty due to the scaling of the events. The solid line is the best fit function for the signal plus background near the endpoint, obtained by using a linear function with Gaussian smearing for the signal and a linear function for the background. The endpoint is extracted to be 179.6 ± 5.8 GeV for M_{llq}. The M_{lq} endpoint cannot be extracted clearly using a simple linear function.

However, with the limited statistics and the narrow physical M_{ll} region of the Higgsino LSP scenario, the threshold of M_{llq} is not quite useful for the mass determination. With fixed M_{ll}^{max} and M_{llq}^{max}, M_{llq}^{min} has a very little sensitivity to the mass parameters.

We therefore have to look for another quantity to determine the three masses. Such a quantity can be obtained by analyzing the squark pair production process followed by the two squarks decaying into two jets and two $\tilde{\chi}_1^0$'s. Although we cannot reconstruct the squark four-momenta due to two escaping invisible neutralinos by the event by event analysis, we can extract a relation between $m_{\tilde{q}}$ and $m_{\tilde{\chi}_1^0}$ by the endpoint analysis of the M_{T2} variable defined in Ref. [63]. This variable is designed to take the maximal value at the squark mass when we input the correct $m_{\tilde{\chi}_1^0}$ in the calculation. The definition is given by

$$M_{T2}^2 = \min_{\mathbf{p}_{T1}^{miss}+\mathbf{p}_{T2}^{miss}=\mathbf{p}_T^{miss}} [\max\{m_T^2(\mathbf{p}_T^{j1}, \mathbf{p}_{T1}^{miss}), m_T^2(\mathbf{p}_T^{j2}, \mathbf{p}_{T2}^{miss})\}],$$

(29)

where $\mathbf{p}_T^{j1}$ and $\mathbf{p}_T^{j2}$ are the transverse momenta of the jets from the squark decays, and $\mathbf{p}_T^{miss}$ is the missing transverse momentum. The transverse mass, m_T^2, is defined by

$$m_T^2(\mathbf{p}_T^a, \mathbf{p}_T^b) = m_a^2 + m_b^2 + 2(E_T^a E_T^b - \mathbf{p}_T^a \cdot \mathbf{p}_T^b).$$

(30)

By identifying the endpoints of M_{T2} for various input values of $m_{\tilde{\chi}_1^0}$, we can obtain a relation between $m_{\tilde{q}}$ and $m_{\tilde{\chi}_1^0}$, which can provide the last information to determine the three masses, $m_{\tilde{\chi}_1^0}$, $m_{\tilde{\chi}_2^0}$ and $m_{\tilde{q}}$.

To select the squark pair production events, we use the following cuts:

(i) $E_T^{miss} > 300$ GeV
(ii) Veto leptons, b-jets, τ-jets
(iii) Two and only two jets with $p_T > 50$ GeV

For our assumptions on the b-tagging and τ-tagging efficiencies, see subsection IVA.

In Fig. 11, we show the M_{T2} distribution for the input value of $m_{\tilde{\chi}_1^0} = 200$ GeV as an example. We can see a clear edge in the distribution around 500 GeV. Fitting with a linear function with a linear background, we obtain the endpoint 505.3 ± 0.6 GeV. With the rich statistics (63 859 events survive the cuts) and the sharp edge, we can measure the endpoint quite accurately. Note that this is not the squark mass itself—it is the value of some quantity that would become the squark mass if our hypothetical input neutralino mass is in fact the true neutralino mass.

Combining the M_{ll}^{max} and M_{llq}^{max} measurements with the M_{T2} analysis, we can now determine all the three masses, $m_{\tilde{q}}$, $m_{\tilde{\chi}_1^0}$ and $m_{\tilde{\chi}_2^0}$, as follows. First, the endpoint analysis of the cascade decay, M_{ll}^{max} and M_{llq}^{max}, gives two constraints on the three mass parameters, leaving one parameter unfixed. If we take this parameter to be $m_{\tilde{\chi}_1^0}$, we can draw a curve on the $m_{\tilde{\chi}_1^0} - m_{\tilde{q}}$ plane, using the constraints from
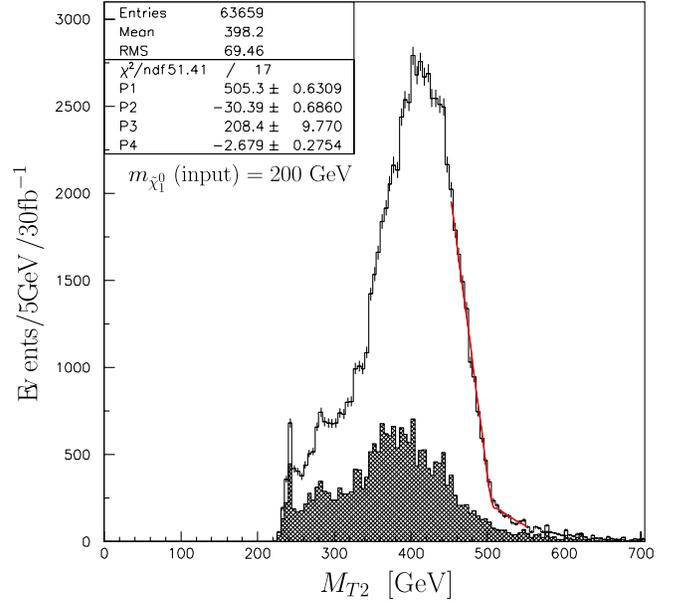
FIG. 11 (color online). The M_{T2} (defined in the text) distribution for the input value of the neutralino mass $m_{\tilde{\chi}_1^0} = 200$ GeV for point I. Hatched histogram is the standard model background. The endpoint is extracted by fitting the signal plus background histogram with a linear function, and the background near the endpoint by a linear function. The endpoint is obtained to be 505.3 ± 0.6 GeV.
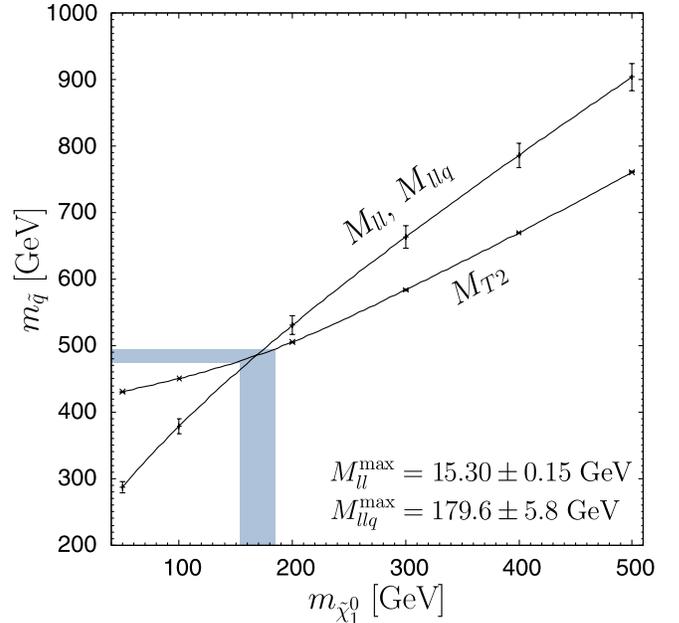
FIG. 12 (color online). Two curves on the $m_{\tilde{\chi}_1^0} - m_{\tilde{q}}$ plane deduced from the cascade decay analysis, M_{ll}^{max} and M_{llq}^{max}, and the squark pair production analysis, M_{T2}^{max}, for point I. Both curves are obtained by inputting hypothetical values of $m_{\tilde{\chi}_1^0}$, which is taken as the horizontal axis. The intersection determines the real values of $m_{\tilde{\chi}_1^0}$ and $m_{\tilde{q}}$. The obtained masses with the 1σ statistical errors are shown by shaded bands.

$M_{ll}^{\max}$ and $M_{llq}^{\max}$. On the other hand, the M_{T2} analysis of the squark pair production gives another relation between $m_{\tilde{\chi}_1^0}$ and $m_{\tilde{q}}$, giving an independent curve on the same plane. The intersection of the two curves will then give the real values of $(m_{\tilde{\chi}_1^0}, m_{\tilde{q}})$. In Fig. 12 we show the two curves explained above with the statistical errors. The M_{T2} curve is obtained by performing the M_{T2} endpoint measurements for six different input values of $m_{\tilde{\chi}_1^0}$ and then interpolating them with a smooth curve. The measured values of $m_{\tilde{\chi}_1^0}$ and $m_{\tilde{q}}$ by this combined analysis are indicated by shaded bands with the 1σ statistical errors.

The effectiveness and accuracy of the method are demonstrated in Fig. 13. To draw the figure, we have generated 10 000 "experiments" and considered that in these experiments the values of $M_{ll}^{\max}$, $M_{llq}^{\max}$ and $M_{T2}^{\max}$ are determined according to the Gaussian distributions with the statistical errors given in Eqs. (25) and (27) and by the M_{T2} fit. We have then calculated the three mass parameters using the method described above and have plotted their distributions. These plots show that $m_{\tilde{\chi}_1^0}$ and $m_{\tilde{q}}$ have larger tails in large mass regions. This represents the fact that the two curves in Fig. 12 are more similar in a larger $m_{\tilde{\chi}_1^0}$ region than in a lower region. The input values of the mass parameters are indicated in Fig. 13 by arrows, and we find that the correct values are obtained within reasonable statistical uncertainties. By fitting the histograms with the Gaussian distribution, we obtain

$$m_{\tilde{\chi}_1^0} = 169 \pm 17 \text{ GeV}, \qquad m_{\tilde{q}} = 486 \pm 11 \text{ GeV},$$
$$\Delta m = 15.30 \pm 0.15 \text{ GeV}. \tag{31}$$

This demonstrates that the neutralino and squark masses can be measured with 10% and 2% level accuracy, respectively, at the LHC in the Higgsino LSP scenario. The mass difference between the two neutral Higgsinos can be mea-

sured at 1% accuracy. The information on these masses are very useful to test particular models, as will be discussed in subsection IV F.

D. Determination of the gluino mass

With the knowledge of the squark and neutralino masses, we can determine the gluino mass using the kinematics of the $\tilde{g} \to \tilde{q}q \to \tilde{\chi}_1^0 qq$ cascade decay. The invariant mass of the two final jets have the maximal value at

$$M_{jj}^{\max} = m_{\tilde{g}}\left(1 - \frac{m_{\tilde{q}}^2}{m_{\tilde{g}}^2}\right)^{1/2}\left(1 - \frac{m_{\tilde{\chi}_1^0}^2}{m_{\tilde{q}}^2}\right)^{1/2}. \tag{32}$$

Therefore, if the endpoint of the M_{jj} distribution arising from this cascade is measured, we can determine the gluino mass.

In supersymmetric models, the gluino production is mostly from the $\tilde{g} + \tilde{q}$ or $\tilde{g} + \tilde{g}$ pair production, which necessarily gives additional jets from the other side of the squark/gluino decay. Those additional jets cause an uncertainty for the selection of the correct jet pair. In order to reduce this combinatorial background, we select the events with three hard jets, which is typical in the $\tilde{g} + \tilde{q}$ production, and choose a pair of jets which gives the smallest M_{jj} among three combinations such that the calculated M_{jj} would not exceed the endpoint in Eq. (32). (Note that this does not mean that the selected pair is necessarily the correct one, but it guarantees that the endpoint of the M_{jj} distribution is given by the right formula, Eq. (32).)

The selection cuts we use are the following:
  (i) $E_T^{\text{miss}} > 300$ GeV
  (ii) Veto leptons, b-jets, τ-jets
  (iii) Three and only three jets with $p_T > 50$ GeV
With these cuts, we obtain the M_{jj} distribution shown in the left panel of Fig. 14. The endpoint structure is visible around 400 GeV. By fitting the histogram near the endpoint
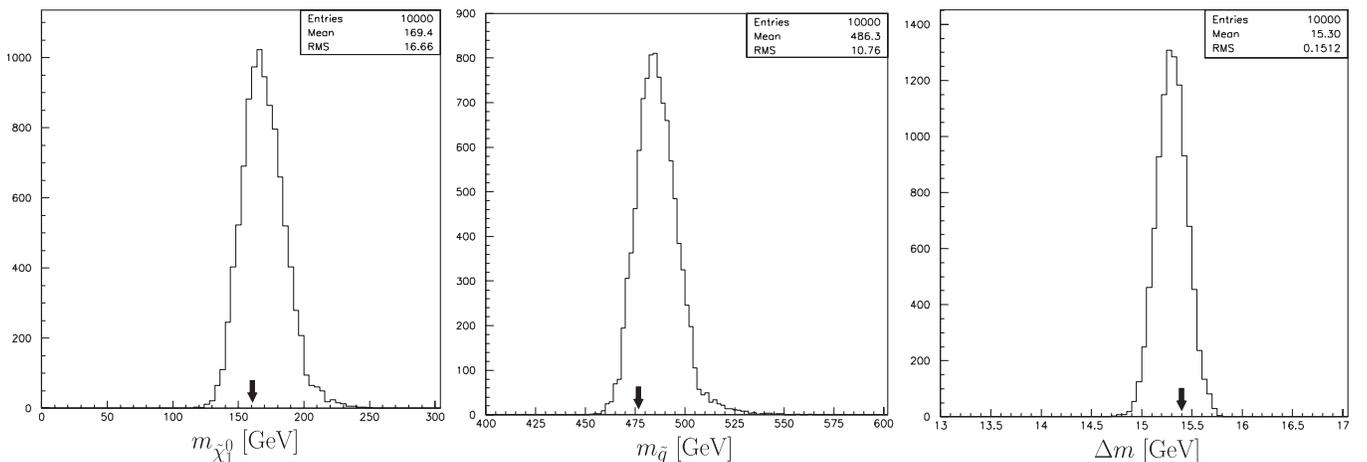
FIG. 13. The statistical errors of the measured mass parameters $m_{\tilde{\chi}_1^0}$, $m_{\tilde{q}}$ and Δm for point I. Arrows indicate the input values used in the Monte Carlo event generation. The accuracy at the level of 10%, 2% and 1% is obtained for $m_{\tilde{\chi}_1^0}$, $m_{\tilde{q}}$ and Δm, respectively.
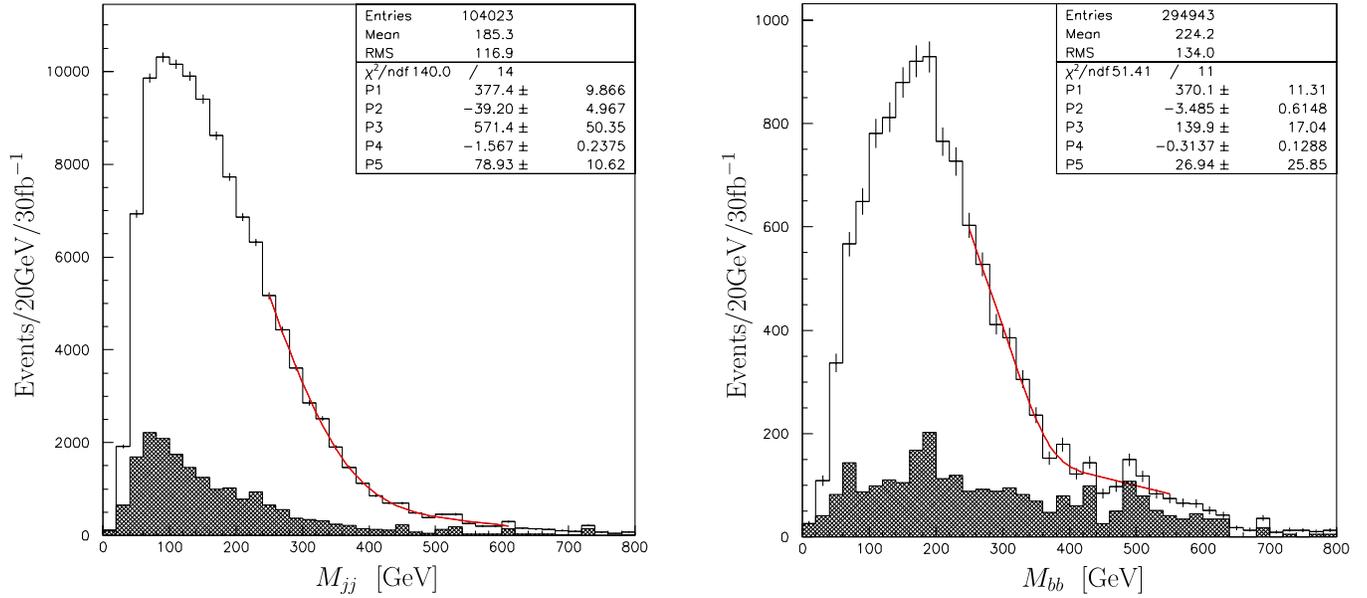
FIG. 14 (color online). The M_{jj} (left) and M_{bb} (right) invariant mass distributions for point I. In the M_{jj} analysis, we select events with three hard jets and take a combination that gives the smallest M_{jj}, out of the three combinations, in order to see the endpoint. A fit is performed with a linear function with Gaussian smearing together with a linear function for the background events. The endpoint is obtained as 377 ± 10 GeV. In the M_{bb} analysis, we select events with three hard jets including two hard b-jets. A similar endpoint, 370 ± 11 GeV, is obtained using the same fitting function.

by a linear function with Gaussian smearing and a linear background shape, we obtain

$$M_{jj}^{\max} = 377 \pm 10 \text{ GeV}. \tag{33}$$

The large value of χ^2 shown in the plot is caused by the artificially magnified statistical uncertainty of the standard model background due to the scaling of the events. We have checked that the reasonable value of χ^2 is obtained without the standard model background.

We can perform the same analysis for the $\tilde{g} \to \tilde{b}b \to \tilde{\chi}_1^0 bb$ decay by requiring two b-jets. We show the resulting M_{bb} distribution in the right panel of Fig. 14. In this case, we do not suffer from the combinatorial background, although the statistics is reduced. If we assume $m_{\tilde{b}} \simeq m_{\tilde{q}}$, which is indeed the case here, we can use this endpoint for the gluino mass reconstruction. We, however, do not use this analysis in the following because it will make our analysis more model-dependent. For the purpose of testing the particular model, however, the M_{bb} analysis can be used as a consistency check (or to extract some information on the value of $\tan\beta$).

Combining the information of $M_{jj}^{\max}$ with the analysis in the last subsection, we can determine the gluino mass. The reconstructed gluino mass is shown in Fig. 15. The input value of $m_{\tilde{g}} = 623$ GeV is indicated by the arrow. We see that the reconstruction is successful within the statistical uncertainty. With the approximation of the statistical fluctuation to take the Gaussian form, we obtain

$$m_{\tilde{g}} = 632 \pm 13 \text{ GeV}. \tag{34}$$

We find that a quite accurate ($\approx 2\%$) measurement of the gluino mass is possible by this method.
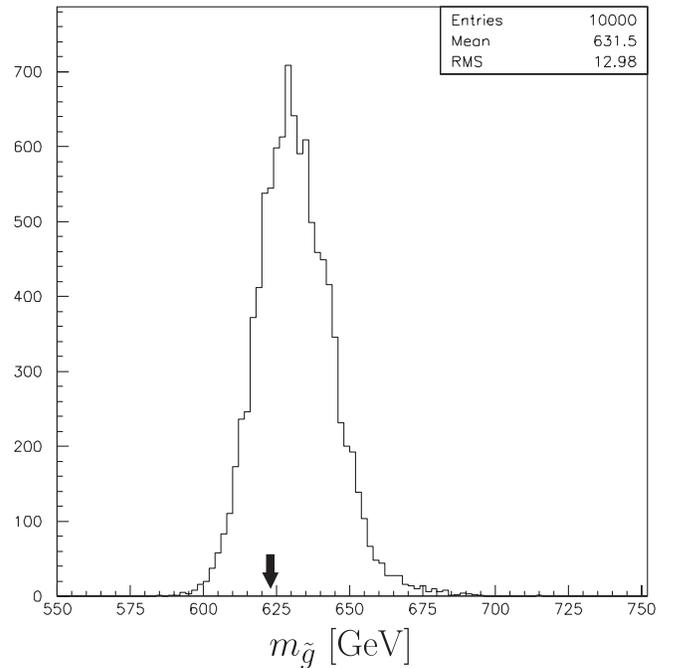
FIG. 15. The statistical error of the gluino mass for point I. The arrow indicates the input value used in the Monte Carlo event generation. The accuracy at the level of 2% is obtained.

There is another method of extracting the gluino mass, which can be used in any model within the class considered here. This is to use the effective mass M_{eff} defined by

$$M_{\text{eff}} = E_T^{\text{miss}} + \sum_i p_T^i, \tag{35}$$

where the sum runs over all the jets. The peak location of this variable is known to have a correlation with the gluino and squark masses [2,3]. In particular, as we will see below, we have a definite relation between the peak location of M_{eff} and the superparticle masses within the model used here. To perform this analysis, we use the cut criteria listed in Ref. [64] to select the events, except for the lepton, b-jet and τ-jet vetoes:

    (i) ≥ 4 jets with $p_T \geq 50$ GeV
    (ii) ≥ 2 jets with $p_T \geq 100$ GeV
    (iii) $E_T^{\text{miss}} \geq \max\{100 \text{ GeV}, 0.25\sum_i p_T^i\}$
    (iv) Transverse sphericity $S_T \geq 0.2$
    (v) $\Delta\phi_{(\mathbf{p}_T^1, \mathbf{p}_T^2)} \leq 170°$
    (vi) $\Delta\phi_{(\mathbf{p}_T^1 + \mathbf{p}_T^2, \mathbf{p}_T^{\text{miss}})} \leq 90°$
    (vii) Veto leptons, b-jets, τ-jets

By generating supersymmetric events for various parameter points in the model, we find an excellent linear relation between $M_{\text{eff}}^{\text{peak}}$ and $m_{\tilde{q}} + m_{\tilde{g}} - m_{\tilde{\chi}_1^0}$ as shown in Fig. 16. The relation is given by

$$M_{\text{eff}}^{\text{peak}} = 285 \text{ GeV} + 0.763(m_{\tilde{q}} + m_{\tilde{g}} - m_{\tilde{\chi}_1^0}). \tag{36}$$
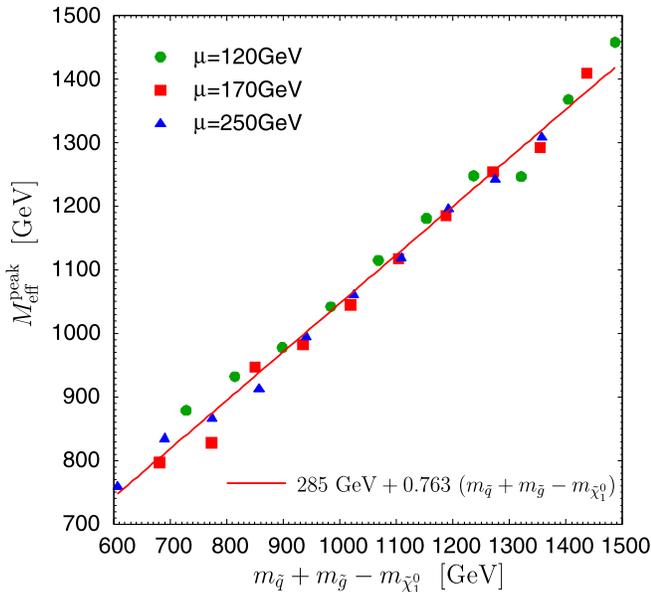
FIG. 16 (color online). An empirical relation between the peak location of M_{eff} and a combination $m_{\tilde{q}} + m_{\tilde{g}} - m_{\tilde{\chi}_1^0}$. We have generated 50 000 events for each 30 sample points in the mixed moduli-anomaly mediation model. A very good linear relation is obtained. Note that this relation will be modified if different selection cuts are used. The standard model background has not been included in searching the peak location.

Note that this should be regarded as a sort of theoretical prediction as we have not included the standard model background in producing the plot. By using this empirical fact, we can extract the combination $m_{\tilde{q}} + m_{\tilde{g}} - m_{\tilde{\chi}_1^0}$ from the M_{eff} peak analysis.

In Fig. 17 we show the distribution of M_{eff} described above. We obtain the peak location $M_{\text{eff}}^{\text{peak}} = 977$ GeV by fitting the histogram near the peak with a Gaussian function. With the assumption that the theoretical relation in Eq. (36) is accurate at a 5% level, we obtain the gluino mass

$$m_{\tilde{g}} = 590 \pm 62 \text{ GeV}, \tag{37}$$

by combining the $M_{\text{eff}}^{\text{peak}}$ analysis here with the analysis in the last subsection. We find that the error amounts to $O(10\%)$. We thus conclude that the M_{jj} endpoint analysis is more useful than the $M_{\text{eff}}^{\text{peak}}$ analysis to determine the gluino mass not only because it is more model-independent but also because it has better accuracy.

E. The case with large superparticle masses

In this subsection we repeat the analyses in subsections IV C and IV D for the case of large superparticle masses (point II in Table I) to see if accurate measurements are still possible despite the smaller statistics due to smaller superparticle production cross sections. The analyses below show that essentially the same method can be used to determine the mass parameters in good
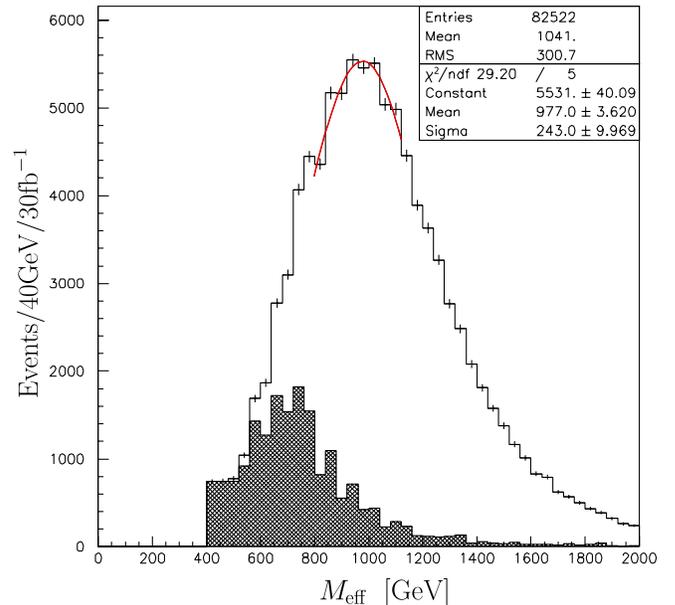
FIG. 17 (color online). The distribution of M_{eff} for point I. The QCD background is smeared in order not to artificially magnify the statistical uncertainty due to the scaling of the events. The location of the peak is determined by fitting with a Gaussian function near the peak. It is given by $M_{\text{eff}}^{\text{peak}} = 977$ GeV.
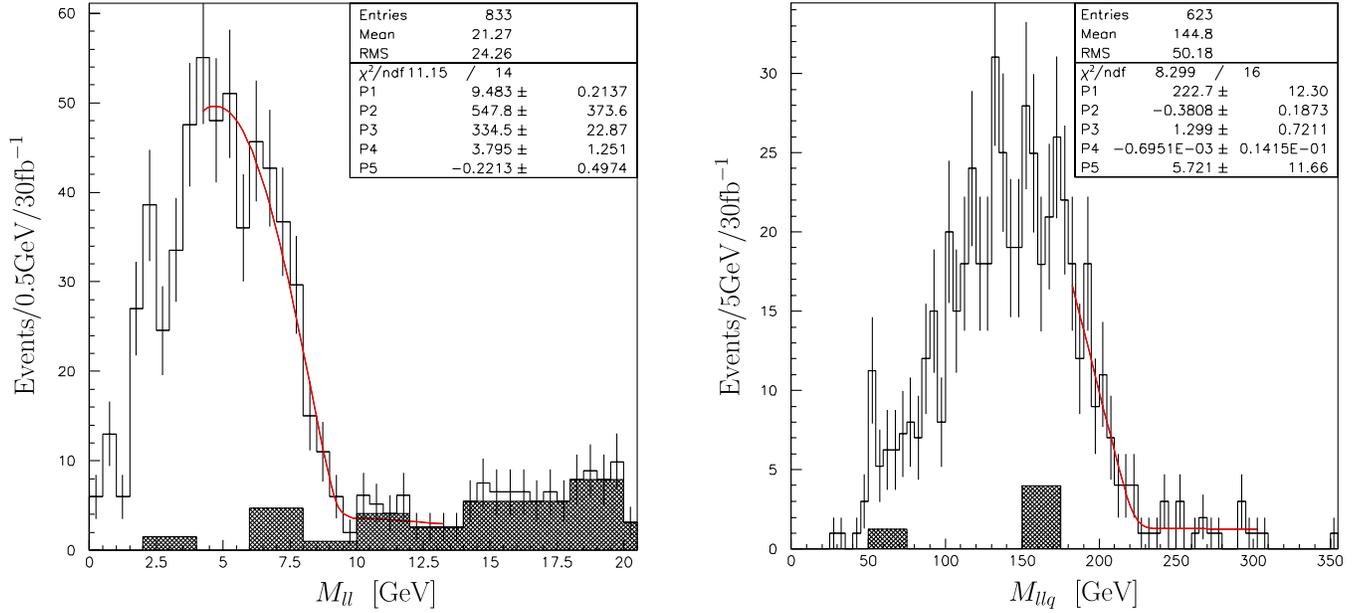
FIG. 18 (color online). The distributions of M_{ll} (left) and M_{llq} (right) for point II. Hatched histogram represents the standard model background, which is smeared over five bins in order not to magnify the statistical uncertainty due to the scaling of the events. For M_{ll}, we have searched the endpoint by fitting with the theoretical curve assuming $\eta_\chi = -1$. The endpoint is obtained to be 9.48 ± 0.21 GeV. For M_{llq}, we have used a linear function with Gaussian smearing for the signal and a linear function for the background. The endpoint is obtained to be 223 ± 12 GeV.

accuracy. In fact, similar or even better accuracy is obtained for the $m_{\tilde{q}}$ and $m_{\tilde{g}}$ determination compared to the case with low superparticle masses, as we will see below.

The M_{ll} and M_{llq} distributions are shown in Fig. 18. We have used the same cuts with those in subsection IV C for the event selection. We can see the clear endpoints in both distributions. The M_{ll} distribution is fitted with the theoretical curve with $\eta_\chi = -1$. A good fit is obtained only for $\eta_\chi = -1$, allowing a successful measurement of η_χ. The endpoints are obtained as:

$$M_{ll}^{\max} = 9.48 \pm 0.21 \text{ GeV}, \qquad M_{llq}^{\max} = 223 \pm 12 \text{ GeV}.$$
$$(38)$$

where the M_{llq} endpoint is determined by a fit using a linear function with Gaussian smearing together with a linear background shape.

The M_{T2} distribution with an input $m_{\tilde{\chi}_1^0} = 200$ GeV is shown in Fig. 19. The signal to background ratio is not so large, but there is no significant background near the endpoint because of the large squark mass. The endpoint measurement, therefore, does not suffer seriously from the standard model background. We obtain 716.6 ± 1.9 GeV for this value of the input neutralino mass. We then repeat the analysis for six different input neutralino masses and obtain a curve on the $m_{\tilde{\chi}_1^0} - m_{\tilde{q}}$ plane by interpolating these points.

The two curves obtained from the M_{ll} and M_{llq} endpoints and the M_{T2} endpoint are shown in Fig. 20. We find
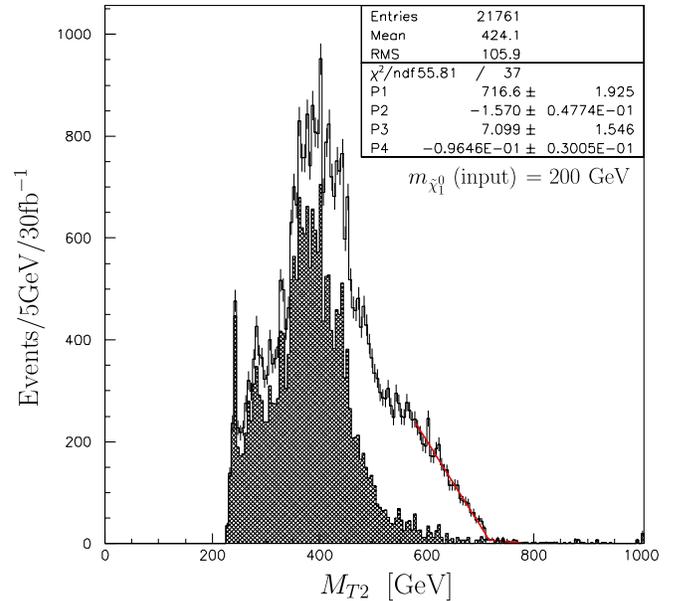
FIG. 19 (color online). The M_{T2} distribution for the input value of the neutralino mass $m_{\tilde{\chi}_1^0} = 200$ GeV for point II. Hatched histogram is the standard model background. The endpoint is extracted by fitting the signal plus background histogram with a linear function, and the background near the endpoint by a linear function. The endpoint is obtained to be 716.6 ± 1.9 GeV.
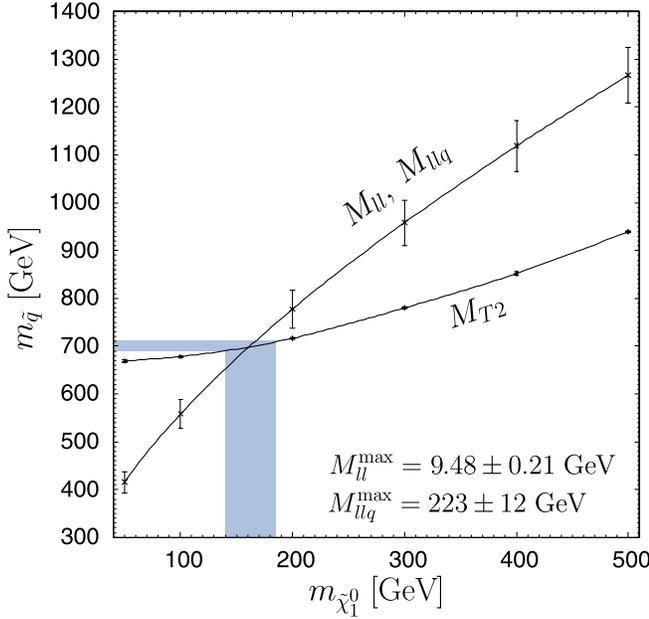
FIG. 20 (color online). Two curves on the $m_{\tilde{\chi}_1^0} - m_{\tilde{q}}$ plane deduced from the cascade decay analysis, $M_{ll}^{\max}$ and $M_{llq}^{\max}$, and the squark pair production analysis, $M_{T2}^{\max}$, for point II. Both curves are obtained by inputting hypothetical values of $m_{\tilde{\chi}_1^0}$. The intersection determines the real values of $m_{\tilde{\chi}_1^0}$ and $m_{\tilde{q}}$. The obtained masses with the 1σ statistical errors are shown by shaded bands.

FIG. 21 (color online). The M_{jj} invariant mass distribution for point II. We select events with three hard jets and take a combination that gives the smallest M_{jj}, out of the three combinations, in order to see the endpoint. A fit is performed with a linear function with Gaussian smearing together with a linear function for the background events. The endpoint is obtained as 609 ± 13 GeV.

that the crossing angle of the curves is larger compared to the case in Fig. 12. This property makes it possible to measure the squark mass in this point with similar accuracy to the case of low superparticle masses, even though we have larger statistical uncertainty.

For the M_{jj} endpoint measurement, we use a different cut for the jet p_T. We take

(i) Three and only three jets with $p_T > 100$ GeV instead of $p_T > 50$ GeV, used in the analysis of the low superparticle mass case, because a clear endpoint is not obtained with the 50 GeV cut. The resulting M_{jj} distribution is shown in Fig. 21. By fitting with a linear function with Gaussian smearing and a linear background, we obtain

$$M_{jj}^{\max} = 609 \pm 13 \text{ GeV}. \tag{39}$$

Combining all the results, we can determine the four mass parameters, $m_{\tilde{\chi}_1^0}$, $m_{\tilde{q}}$, Δm and $m_{\tilde{g}}$. The estimation of the statistical uncertainties is given in Fig. 22. The input values are indicated with the arrows, which are all within reasonable statistical uncertainties. The gluino mass is obtained with slightly larger values. This is caused by the systematics that the M_{jj} endpoint tends to give larger values than the one obtained in Eq. (32) when we use the $p_T > 100$ GeV cut for jets. Therefore, the estimation of the systematic error will be important in this analysis. By

fitting the histograms with Gaussian functions, we obtain

$$m_{\tilde{\chi}_1^0} = 164 \pm 24 \text{ GeV}, \qquad m_{\tilde{q}} = 700 \pm 12 \text{ GeV},$$
$$\Delta m = 9.5 \pm 0.2 \text{ GeV}, \tag{40}$$

$$m_{\tilde{g}} = 940 \pm 15 \text{ GeV}. \tag{41}$$

The neutralino, squark and gluino masses can be measured at 15%, 2% and 2% level accuracy, respectively. Since this point represents the case of the highest superparticle masses from the naturalness requirement (see Eq. (23)), the above analysis shows that the method of mass determination developed here covers the entire region of the parameter space.

For completeness, we show in Fig. 23 the M_{eff} distribution. The standard model background is huge, although it is not so significant around the peak location. By using the relation in Eq. (36), we obtain the gluino mass

$$m_{\tilde{g}} = 801 \pm 85 \text{ GeV}, \tag{42}$$

which is slightly deviated from the input value of 917 GeV (by 1.4σ). This little discrepancy is mainly caused by the shift of M_{eff} in the lower direction due to the standard model background. For a realistic use of the M_{eff} analysis in the high superparticle mass region, one needs to develop a better understanding of the shape of the standard model background and/or to devise a better cut (especially on E_T^{miss}) to reduce the standard model background. Note that
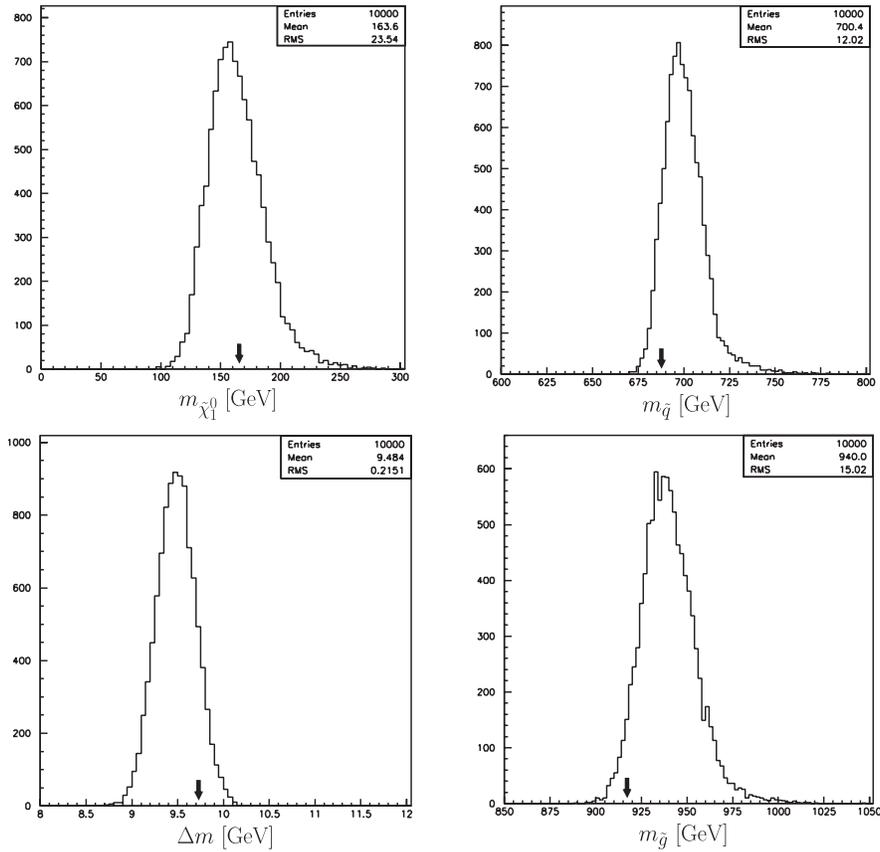
FIG. 22. The statistical errors of the measured mass parameters $m_{\tilde{\chi}_1^0}$, $m_{\tilde{q}}$, Δm and $m_{\tilde{g}}$ for point II. Arrows indicate the input values used in the Monte Carlo event generation. The accuracy at the level of 15%, 2%, 2% and 2% is obtained for $m_{\tilde{\chi}_1^0}$, $m_{\tilde{q}}$, Δm and $m_{\tilde{g}}$, respectively.

the relation in Eq. (36) will be modified if different cuts are used.

F. Testing the model with mixed moduli-anomaly mediation

One of the most important features of the LHC experiment is its potential of ruling out models. With the limited precisions of various measurements, it is extremely important to develop methods of testing model predictions rather than just measuring parameters under the assumption of a particular model. We here take the model with mixed moduli-anomaly mediation as an example and discuss possible ways of testing the model.

We have already seen that one of the characteristic features, the Higgsino LSP, can be tested using the distribution of the dilepton invariant mass from $\tilde{\chi}_2^0$ decay. Other interesting features of the model include approximate universality of the gaugino masses and the definite ratio between the sfermion and gaugino masses, given in Eq. (22). We can test these features by using the mass parameters obtained in the previous analyses. Specifically, we can calculate the parameter M_0 in three different ways and compare them with each other. If the relations pre-
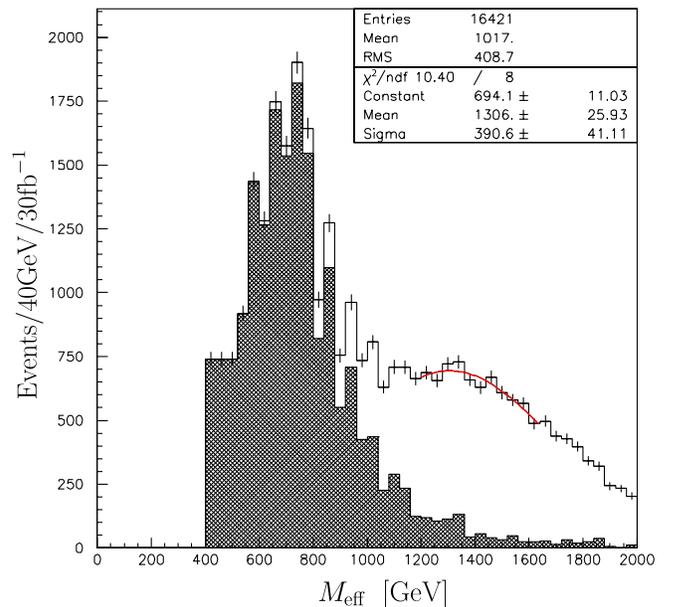
FIG. 23 (color online). The $M_{\rm eff}$ distribution for point II. The QCD background is smeared in order not to artificially magnify the statistical uncertainty due to the scaling of the events. The peak location is determined by fitting with a Gaussian function near the peak. It is found to be $M_{\rm eff}^{\rm peak} = 1306$ GeV.

dicted in the model hold, the three values must coincide within (mostly theoretical) uncertainties/corrections.

The first way of calculating M_0 is to use the measured neutralino mass difference, Δm. By using Eq. (16) with $M_1 \simeq M_2 \simeq M_0$, we can extract M_0 as

$$M_0 \simeq \frac{m_Z^2}{\Delta m}. \tag{43}$$

This must give the correct value of M_0 up to corrections of $\approx 15\%$, which come mainly from $O(|\mu| \sin 2\beta / M_0)$ corrections in diagonalizing the neutralino mass matrix and from the effect of running between the effective messenger scale, M_{mess}, and the gaugino mass scale. The other two ways use direct measurements of the squark and gluino masses:

$$M_0 \simeq \sqrt{2} m_{\tilde{q}}, \qquad M_0 \simeq m_{\tilde{g}}, \tag{44}$$

which must also give the correct value of M_0 up to corrections. The corrections come, for example, from running between M_{mess} and the superparticle mass scale as well as from finite supersymmetric QCD corrections. For the squark masses, the $SU(2)_L$ and $U(1)_Y$ D-terms also give corrections of $O(m_Z^2 / M_0^2)$. All these corrections, again, amount to $\approx 15\%$. We thus conclude that the three values of M_0 calculated using Eqs. (43) and (44) must coincide within 15%, if the model is actually realized. This can provide a rather nontrivial test for the model.

We show in Fig. 24 the values of M_0 calculated in three different ways for point I ($M_0 = 600$ GeV; left panel) and for point II ($M_0 = 900$ GeV; right panel). The shaded regions indicate the $\pm 15\%$ range around the true values of M_0 (= 600 GeV and 900 GeV). For $m_{\tilde{g}}$, we have plotted both values obtained from the M_{jj} endpoint and the M_{eff} peak analyses. As we can see, all measurements agree with each other within 15% uncertainties, both for the cases of point I and point II. Moreover, we can even understand a nature of the dispersions in the plot. We find that the $O(|\mu| \sin 2\beta / M_0)$ correction to $m_Z^2 / \Delta m$ is negative

whereas the QCD corrections to the squark and gluino masses are positive, as expected from theory. Since experimental errors on determining these quantities are rather small, the structure of these dispersions might be useful for deducing further detailed structures of the underlying theory, such as the structure of higher order corrections to the superparticle masses.

V. DISCUSSION AND CONCLUSIONS

Weak scale supersymmetry is often said to be fine-tuned, especially if the matter content is minimal. Is it true? If the LEP II bound on the Higgs boson mass pushed the top squark masses above a TeV, as is sometimes stated in literature, this would be a true statement. The size of the top-stop loop contribution to the Higgs boson mass-squared parameter, $m_{H_u}^2$, would then be larger than about $(250 \text{ GeV})^2$ even for a unit logarithm, $\ln(M_{\text{mess}}/m_{\tilde{t}}) \approx 1$, leading to fine-tuning of order 10% *independently of* an underlying mechanism of supersymmetry breaking (see Eqs. (2) and (3)). In fact, in most supersymmetry breaking models, the logarithm is (much) larger than 1, leading to (much) severer fine-tuning. For example, fine-tuning is already as bad as 2% for $M_{\text{mess}} \approx 100$ TeV. Such heavy top squarks, therefore, would not allow natural electroweak symmetry breaking in the context of minimal supersymmetry.

The situation, however, is not as described above if there is a large A_t term at the weak scale. For $|A_t/m_{\tilde{t}}| \approx (1.5 \sim 2.5)$, the top squark masses can be as small as $m_{\tilde{t}} \approx (250 \sim 400)$ GeV to evade the LEP II constraint of $M_{\text{Higgs}} \gtrsim 114.4$ GeV, so that the "model-independent" contribution to $m_{H_u}^2$ from top-stop loop is only about $(100 \text{ GeV})^2$, even including the contribution from the A_t term. (The lower bound on $m_{\tilde{t}}$ here, ≈ 250 GeV, arises in fact from the direct search bound of the top squark, $m_{\tilde{t}_1} \gtrsim 100$ GeV, and not from the Higgs boson mass bound.) Such light top squarks allow "fine-tuning" to be only of $O(20\%)$ for $M_{\text{mess}} = O(10 \text{ TeV})$ and allow completely natural electro-
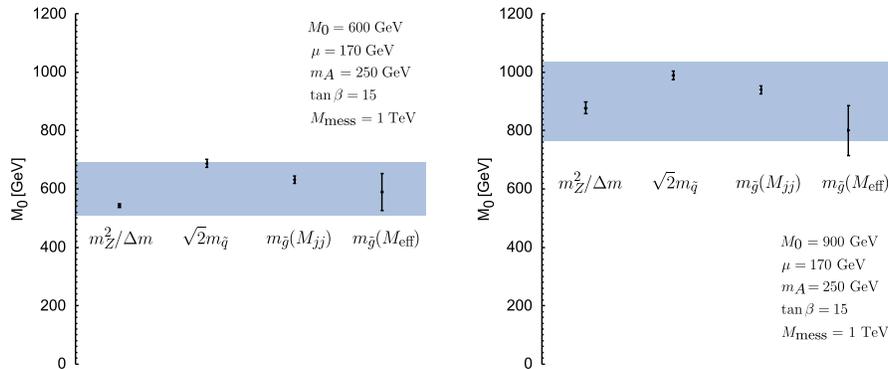
FIG. 24 (color online). A nontrivial test for the mixed moduli-anomaly mediation model in the case of $M_0 = 600$ GeV (left) and $M_0 = 900$ GeV (right). Three ways of calculating M_0, i.e. $m_Z^2/\Delta m$, $\sqrt{2} m_{\tilde{q}}$ and $m_{\tilde{g}}$, give the same value within $\approx 15\%$ theoretical uncertainties. For $m_{\tilde{g}}$, we have plotted the values obtained in two different ways, i.e. from M_{jj}^{max} and $M_{\text{eff}}^{\text{peak}}$.

weak symmetry breaking for smaller values of $M_{\rm mess}$. With these low-energy spectra, the amount of fine-tuning, Δ^{-1}, can also be small for theories with large logarithms. We find that $\Delta^{-1} \approx 10\%$ is possible even in theories with $M_{\rm mess} \sim M_{\rm unif}$. Therefore, under the current experimental constraints, the supersymmetric fine-tuning problem should *not* be regarded as the problem of minimal supersymmetry itself but as the problem of specific supersymmetry-breaking mechanisms.

Characteristic features required to have (relatively) natural electroweak symmetry breaking in minimal supersymmetric theories are (i) a large A term for the top squarks, $|A_t/m_{\tilde{t}}| \approx (1.5 \sim 2.5)$ (ii) light top squarks (iii) a moderately large ratio of the electroweak VEVs, $\tan\beta \gtrsim 5$, and (iv) a small μ term, $|\mu| \lesssim 190$ GeV (270 GeV) for $\Delta^{-1} \gtrsim 20\%$ (10%). A generic implication of these low-energy spectra is a relatively light Higgs boson, $M_{\rm Higgs} \lesssim 120$ GeV. There will be classes of theories leading to these features/spectra, and we have identified two representative ones (see Fig. 5). Among them, a class giving nearly universal gaugino and sfermion masses at low energies [see Fig. 5(b)] can make electroweak symmetry breaking most natural. Examples for these theories are obtained by employing moduli-type, or boundary condition, supersymmetry breaking (effectively) at a low scale. A consistency with the desert can be explicitly recovered if the setup is realized through mixed moduli and anomaly mediated supersymmetry breaking.

An important consequence of the class of theories described above is that the Higgsinos are the lightest among the superpartners of the standard model particles. Assuming that the gravitino is not much lighter than the Higgsinos, which is actually the case in the model with mixed moduli-anomaly mediation, the existence of the nearly degenerate Higgsino states ($\tilde{\chi}_1^0$, $\tilde{\chi}_2^0$ and $\tilde{\chi}_1^+$) can give interesting signals at the LHC. The signals arise in the invariant mass distribution of dileptons arising from $\tilde{\chi}_2^0$ decay: a smallness of the endpoint and a particular shape determined by the relative CP property of the two neutralinos, $\tilde{\chi}_1^0$ and $\tilde{\chi}_2^0$. We have argued that these signals are indeed useful in a wide variety of circumstances within the class of theories considered here.

We have explicitly demonstrated the usefulness of the signals in realistic analyses by performing Monte Carlo simulations, including detector simulations and background estimations. We have also presented a method that allows the determination of all the relevant superparticle masses, $m_{\tilde{\chi}_1^0}$, $m_{\tilde{q}}$, $m_{\tilde{g}}$ and $\Delta m = m_{\tilde{\chi}_2^0} - m_{\tilde{\chi}_1^0}$, independently of the details of the model. This allows us to determine all the superparticle masses within the class of models considered, up to *theoretical* uncertainties of $\approx 15\%$. Note that some of the existing techniques, e.g. the M_{llq} threshold analysis, is not very useful here because of the near degeneracy of the Higgsino states. We can, nevertheless, determine the four mass parameters with the pre-

cisions of order a few to 10%, by combining various endpoint analyses. This is extremely important because it provides ways to test various possible models, which generically give nontrivial relations among these parameters. We have demonstrated this in the case of the model with mixed moduli-anomaly mediation, and shown that the model can indeed be tested (and thus can be discriminated from models that give significantly different relations among the four parameters).

It will be possible to perform further tests for the class of models discussed here. An important issue is to measure the A parameters, especially that of the top squarks. This may be done, for example, along the lines presented in [65]. There is also an important interplay between collider physics and cosmology. As discussed in Ref. [11], the present class of models has a large discovery potential in ongoing and future direct dark matter detection experiments, such as CDMS II, if the Higgsino LSP composes the dark matter of the universe. Now suppose that the mass and the detection cross section for the dark matter are measured in (one of) these experiments. The results from the LHC can then be used to perform a consistency check on the LSP mass and to provide a constraint on the Higgs sector parameters, m_A and $\tan\beta$, because the detection cross section depends strongly on these parameters. Together with the other data from the LHC, such as the one for the Higgs boson mass, we will be able to determine all the parameters of the model with certain accuracy.

In performing all these analyses, inputs from a particular model(s) will be very important/useful, especially if one wants to pin down the parameter point of minimal weak scale supersymmetry. The model(s) assumed is then better to be a "likely" one, compared with other possible models that can also "accommodate" the same set of measurements. Naturalness of electroweak symmetry breaking, together with the simplicity of a model, will then keep playing an important guiding role in these "model selection" processes, which will most likely take the form of processes of "slowly convincing ourselves."

APPENDIX A: RENORMALIZATION GROUP PROPERTIES OF MODULI MEDIATION MODELS

We here study interesting renormalization group (RG) properties of moduli mediated supersymmetry-breaking models. It is found in Ref. [48] that mixed moduli-anomaly

mediation models have an interesting RG property—the contributions from anomaly mediation can be canceled by the actual one-loop running effect at a certain energy scale, mimicking a pure moduli mediated model at that energy scale. Since a clear derivation of the result is not available in the paper, we present it here. We show that the result can be understood as a rather straightforward consequence of special properties of moduli mediated models. We use the method of "analytic continuation into superspace" [66], which provides a powerful way of analyzing RG equations in softly broken supersymmetric theories. We explain the basic mechanism of this interesting property and the origin of the conditions for the cancellation to happen. We also point out that the effects of mass thresholds are under a good theoretical control.

We consider the case where the effective Lagrangian is given at a scale Λ as follows:

$$\mathcal{L} = \int d^4\theta (T + T^\dagger)^{r_i} Q_i^\dagger e^{-2V} Q_i + \left(\int d^2\theta \frac{\lambda_{ijk}}{6} Q_i Q_j Q_k \right.$$
$$\left. + \text{h.c.} \right) + \left(\int d^2\theta T \mathcal{W}^\alpha \mathcal{W}_\alpha + \text{h.c.} \right), \quad \text{(A1)}$$

where T is a spurion field with a nonvanishing F-component. This is the form of the Lagrangian obtained in moduli (radion) mediated models. The lowest component of T represents the volume of the extra dimensions in which the gauge fields propagate. The rational number r_i represents how much fraction of the extra dimensions the matter Q_i propagates, compared with the gauge fields. For example, if the gauge fields and the matter field Q_i propagate in six and five dimensional spacetime, respectively, r_i is given by $(5 - 4)/(6 - 4) = 1/2$.

We now exploit the following property of moduli mediated models to show certain special RG properties of these models. We first note that at tree level there are following simple scaling relations associated with the rescaling of the moduli field T:

$$S \to aS, \qquad Z_i \to a^{r_i} Z_i \quad \text{for } T \to aT, \quad \text{(A2)}$$

where S and Z_i are the gauge kinetic function and the wavefunction factor defined by $\mathcal{L} \ni [S \mathcal{W}^\alpha \mathcal{W}_\alpha]_F$ and $\mathcal{L} \ni [Z_i Q_i^\dagger Q_i]_D$, respectively. We then find that these scaling relations can be extended to the one-loop level if the moduli rescaling, $T \to aT$, is supplemented by the following rescalings of the RG scale μ_R and the Yukawa couplings:

$$\ln\frac{\mu_R}{\Lambda} \to a \ln\frac{\mu_R}{\Lambda}, \qquad \lambda_{ijk} \to a^{(r_i+r_j+r_k-1)/2} \lambda_{ijk}, \quad \text{(A3)}$$

where λ_{ijk} are the superpotential Yukawa couplings appearing in Eq. (A1) (the "physical" Yukawa couplings are given by $y_{ijk} \equiv \lambda_{ijk}/(Z_i Z_j Z_k)^{1/2}$). Once this property is proved (see later), we can use these scaling relations to show that the gauge kinetic function, S, and the wavefunction factor, Z_i, take the following form:

$$S = T \cdot \hat{S}\left(\frac{\ln(\mu_R/\Lambda)}{T}\right), \quad \text{(A4)}$$

$$Z_i = (T + T^\dagger)^{r_i} \cdot \hat{Z}_i\left(\frac{|\lambda_{ijk}|^2}{(T + T^\dagger)^{r_i+r_j+r_k-1}}, \frac{1}{T + T^\dagger} \ln\frac{\mu_R^2}{|\Lambda|^2}\right), \quad \text{(A5)}$$

at an arbitrary scale μ_R. Here, $\hat{S}$ and $\hat{Z}_i$ are some functions, and we have used the fact that Z_i can depend only on T through the combination $T + T^\dagger$ because of the invariance of the Lagrangian under the transformation $T \to T + i\beta$.

Now, suppose that the condition $r_i + r_j + r_k = 1$ is satisfied for the fields having the Yukawa interaction λ_{ijk}. We then find that the T dependencies in $\hat{S}$ and $\hat{Z}_i$ appear only with the renormalization scale μ_R. In this case, the gaugino masses, A terms, and soft scalar squared masses are simply given by:

$$m_\lambda = \frac{1}{2}[\ln S]_F = M_0\left[1 + \frac{2bg^2}{(4\pi)^2} \ln\frac{\mu_R}{\Lambda} \right], \quad \text{(A6)}$$

$$A_{ijk} = -([\ln Z_i]_F + [\ln Z_j]_F + [\ln Z_k]_F)$$
$$= -M_0\left[1 + 2(\gamma_i + \gamma_j + \gamma_k) \ln\frac{\mu_R}{\Lambda} \right], \quad \text{(A7)}$$

$$m_i^2 = -[\ln Z_i]_D = M_0^2\left[r_i + 4\gamma_i \ln\frac{\mu_R}{\Lambda} + 2\dot{\gamma}_i\left(\ln\frac{\mu_R}{\Lambda} \right)^2 \right], \quad \text{(A8)}$$

at an arbitrary renormalization scale μ_R. Here, g and b represent the gauge couplings and the beta function coefficients, $d\ln(1/g^2)/d\ln\mu_R = -2b/(4\pi)^2$, respectively, and γ_i and $\dot{\gamma}_i$ are the anomalous dimensions, $d\ln Z_i/d\ln\mu_R = -2\gamma_i$, and their derivatives with respect to the scale μ_R, $\dot{\gamma}_i = d\gamma_i/d\ln\mu_R$. The overall supersymmetry-breaking parameter M_0 is defined by

$$M_0 = \frac{[T]_F}{[T + T^\dagger]_A}, \quad \text{(A9)}$$

where the subscript A denotes the lowest component. Note that the soft supersymmetry-breaking parameters in Eqs. (A6)–(A8) are given by simple functions of the quantities at the scale μ_R, the gauge couplings, beta functions and anomalous dimensions, as well as $\ln(\mu_R/\Lambda)$.

It is rather simple to prove the scaling relations in Eqs. (A2) and (A3). The RG equations for the gauge couplings (the gauge kinetic functions $S = 1/2g^2 + \cdots$) are given by

$$\frac{d}{dt} S(T, t) = -\frac{b}{(4\pi)^2}, \quad \text{(A10)}$$

where we have defined $t \equiv \ln(\mu_R/\Lambda)$. This obviously leads to

$$\frac{d}{dt}S(T, t) = \frac{d}{d(at)}aS(T, t) = -\frac{b}{(4\pi)^2}. \qquad \text{(A11)}$$

On the other hand, the RG equations for $S(aT, at)$ are given by

$$\frac{d}{d(at)}S(aT, at) = -\frac{b}{(4\pi)^2}. \qquad \text{(A12)}$$

We thus find that $aS(T, t)$ satisfies the same RG equation as $S(aT, at)$. With the initial condition $S(T, 0) = T$, we can determine the integration constant:

$$S(aT, at) = aS(T, t). \qquad \text{(A13)}$$

This implies that S scales as $S \to aS$ for $(T, t) \to (aT, at)$, which is the relation we wanted to prove. In fact, the result here is not a special property of moduli mediated models. The effective Lagrangian in softly broken supersymmetric theories can always be recast in the form of Eq. (A1) as far as the gauge sector is concerned, so that the expression for the gaugino masses in Eq. (A6) is a (well-known) general result.

We can prove the scaling properties of Z_i's along the same lines. The RG equations for Z_i's are

$$\frac{d}{dt}\ln Z_i = -2\gamma_i = \frac{1}{2}\sum_{j,k}\frac{|\lambda_{ijk}|^2}{Z_iZ_jZ_k} - 2(S + S^\dagger)^{-1}C_2^{(i)}(R), \qquad \text{(A14)}$$

at one loop, where $C_2^{(i)}(R)$ is the quadratic Casimir operator for the superfield Q_i.[9] We can again transform this to

$$\begin{aligned}\frac{d}{d(at)}\ln(a^{r_i}Z_i) &= \frac{1}{2}\sum_{j,k}\frac{a^{-1}|\lambda_{ijk}|^2}{Z_iZ_jZ_k} - 2a^{-1}(S(T, t) \\ &\quad + S(T, t)^\dagger)^{-1}C_2^{(i)}(R) \\ &= \frac{1}{2}\sum_{j,k}\frac{a^{r_i+r_j+r_k-1}|\lambda_{ijk}|^2}{(a^{r_i}Z_i)(a^{r_j}Z_j)(a^{r_k}Z_k)} \\ &\quad - 2(S(aT, at) + S(aT, at)^\dagger)^{-1}C_2^{(i)}(R), \end{aligned} \qquad \text{(A15)}$$

where we have used Eq. (A13) in the second equation. This equation shows that $a^{r_i}Z_i(T, \lambda_{ijk}, t)$ satisfies the same RG equation as $Z_i(aT, a^{(r_i+r_j+r_k-1)/2}\lambda_{ijk}, at)$. With the initial condition of $Z_i(T, \lambda_{ijk}, 0) = (T + T^\dagger)^{r_i}$, the integration constant is determined and we obtain

$$Z_i(aT, a^{(r_i+r_j+r_k-1)/2}\lambda_{ijk}, at) = a^{r_i}Z_i(T, \lambda_{ijk}, t). \qquad \text{(A16)}$$

This is the scaling relation for Z_i given in Eqs. (A2) and (A3).

---

[9]Precisely speaking, $S + S^\dagger$ in Eq. (A14) should be the real gauge coupling superfield R defined by $R - (T_G/8\pi^2)\ln R = S + S^\dagger - \sum_i(T_i/8\pi^2)\ln Z_i$ (in the NSVZ scheme). The difference, however, is irrelevant at the one-loop level.

There is a subtlety if the gauge group contains a $U(1)$ factor. In this case the Fayet-Iliopoulos term

$$\int d^4\theta \xi V_Y, \qquad \text{(A17)}$$

may be induced at one loop, which contributes to the soft scalar squared masses as

$$m_i^2 = -[\ln Z_i]_D + g_Y^2\xi Y_i, \qquad \text{(A18)}$$

where g_Y is the $U(1)$ gauge coupling and Y_i is the $U(1)$ charge of the superfield Q_i. The RG equation for ξ is given by [67]

$$\frac{d}{dt}\xi = \frac{-2}{(4\pi)^2}\left[\sum_i Y_i\ln Z_i\right]_D + \frac{2g_Y^2}{(4\pi)^2}\xi\sum_i Y_i^2. \qquad \text{(A19)}$$

Since the combination of $\sum_i Y_i\ln Z_i$ is RG invariant, i.e. $\sum_i Y_i\gamma_i = 0$, ξ is never generated if $\sum_i Y_i\ln Z_i = 0$ (and $\xi = 0$) at the classical level. Therefore, we can neglect the contributions to m_i^2 from the Fayet-Iliopoulos term if the condition $\sum_i Y_i r_i = 0$ is satisfied.

In the case where there is a mass threshold M, we find that the scaling properties of Eqs. (A2) and (A3) are maintained if the rescalings of T, μ_R and λ_{ijk} are supplemented by

$$\ln\frac{M}{\Lambda} \to a\ln\frac{M}{\Lambda}. \qquad \text{(A20)}$$

The functions $\hat{S}$ and $\hat{Z}_i$, in this case, can depend on $\ln(M/\Lambda)/T$ and $\ln(|M|^2/|\Lambda|^2)/(T + T^\dagger)$, respectively. The soft supersymmetry-breaking terms, therefore, obtain additional contributions:

$$\Delta m_\lambda = \frac{2\Delta b g^2}{(4\pi)^2}M_0\ln\frac{M}{\Lambda}, \qquad \text{(A21)}$$

$$\Delta A_{ijk} = -2(\Delta\gamma_i + \Delta\gamma_j + \Delta\gamma_k)M_0\ln\frac{M}{\Lambda}, \qquad \text{(A22)}$$

$$\Delta m_i^2 = M_0^2\left[4\Delta\gamma_i\ln\frac{M}{\Lambda} + 2\Delta\dot{\gamma}_i\left(\ln\frac{M}{\Lambda}\right)^2\right], \qquad \text{(A23)}$$

where Δb, $\Delta\gamma_i$ and $\Delta\dot{\gamma}_i$ are the changes of b, γ_i and $\dot{\gamma}_i$ at the scale M ((high scale value) − (low scale value)). The gauge coupling g in Eq. (A21) is the one at the scale μ_R.

The derivation here should make it clear the origins of the special properties of Eqs. (A6)–(A8) and the required condition $r_i + r_j + r_k = 1$. Since the RG equations for the gauge and Yukawa couplings take the form of $dg/dt \sim g^3$ and $dy/dt \sim y^3 + yg^2$ at one loop, and $g^2 \propto 1/T$ and $y^2 \propto (Z_iZ_jZ_k)^{-1} \propto (T + T^\dagger)^{-(r_i+r_j+r_k)}$ in moduli mediated models, it is clear that one-loop RG equations are invariant under the rescaling $(T, t) \to (aT, at)$ if $r_i + r_j + r_k = 1$ is chosen. This scaling property then guarantees the forms of Eqs. (A4) and (A5), leading to Eqs. (A6)–(A8). (This also makes it clear that these properties persist under the ex-

istence of arbitrary generational mixings.) This simple scaling property clearly cannot persist at higher loop orders, so that the properties of Eqs. (A6)–(A8) are that of one-loop RG equations.

Inclusion of anomaly mediation is straightforward at this point. We should simply replace Λ in Eqs. (A4) and (A5) by $\Lambda\Phi$, where $\Phi(= 1 + m_{3/2}\theta^2)$ is the chiral compensator field. (Note that the compensator field Φ does not couple to T as T is a dimensionless chiral superfield.) A curious similarity between moduli and anomaly mediations is manifest here. In particular, at the scale

$$\ln\frac{\Lambda}{\mu_R} = \frac{m_{3/2}}{2M_0}, \qquad (A24)$$

the F-component of $\ln(\mu_R/\Lambda\Phi)/T$ as well as F- and D-components of $\ln(\mu_R^2/|\Lambda\Phi|^2)/(T + T^\dagger)$ vanish. Therefore, either $\hat{S}$ or $\hat{Z}$ does not have F- or D-components if the condition $r_i + r_j + r_k = 1$ is satisfied. The solutions of the RG equations at this scale are remarkably simple:

$$m_\lambda = M_0, \qquad A_{ijk} = -M_0, \qquad m_i^2 = r_i M_0^2. \quad (A25)$$

If there is a mass threshold, the solutions are obtained by simply adding the contributions in Eqs. (A21)–(A23), because of the ultraviolet insensitivity of anomaly mediated contributions.

[1] LEP Collaborations, LEP Electroweak Working Group, and SLD Electroweak and Heavy Flavour Groups, hep-ex/0509008.

[2] H. Baer, C. h. Chen, F. Paige, and X. Tata, Phys. Rev. D **52**, 2746 (1995); **53**, 6241 (1996).

[3] I. Hinchliffe, F. E. Paige, M. D. Shapiro, J. Soderqvist, and W. Yao, Phys. Rev. D **55**, 5520 (1997); H. Bachacou, I. Hinchliffe, and F. E. Paige, Phys. Rev. D **62**, 015009 (2000).

[4] H. Baer, C. h. Chen, M. Drees, F. Paige, and X. Tata, Phys. Rev. D **59**, 055014 (1999); D. Denegri, W. Majerotto, and L. Rurua, Phys. Rev. D **60**, 035008 (1999); I. Hinchliffe and F. E. Paige, Phys. Rev. D **61**, 095011 (2000).

[5] I. Hinchliffe and F. E. Paige, Phys. Rev. D **60**, 095002 (1999).

[6] ATLAS Detector and Physics Performance Technical Design Report, Chap. 20, http://atlas.web.cern.ch/Atlas/GROUPS/PHYSICS/TDR/access.html.

[7] B. C. Allanach, C. G. Lester, M. A. Parker, and B. R. Webber, J. High Energy Phys. 09 (2000) 004.

[8] G. Weiglein *et al.* (LHC/LC Study Group), hep-ph/0410364.

[9] R. Kitano and Y. Nomura, Phys. Lett. B **631**, 58 (2005).

[10] K. Choi, K. S. Jeong, T. Kobayashi, and K. i. Okumura, Phys. Lett. B **633**, 355 (2006).

[11] R. Kitano and Y. Nomura, Phys. Lett. B **632**, 162 (2006).

[12] M. Bastero-Gil, C. Hugonie, S. F. King, D. P. Roy, and S. Vempati, Phys. Lett. B **489**, 359 (2000); K. Agashe and M. Graesser, Nucl. Phys. **B507**, 3 (1997).

[13] J. L. Feng, K. T. Matchev, and T. Moroi, Phys. Rev. Lett. **84**, 2322 (2000); Phys. Rev. D **61**, 075005 (2000).

[14] A. Brignole, J. A. Casas, J. R. Espinosa, and I. Navarro, Nucl. Phys. **B666**, 105 (2003); **B666**, 105 (2003); J. A. Casas, J. R. Espinosa, and I. Hidalgo, J. High Energy Phys. 01 (2004) 008.

[15] P. Batra, A. Delgado, D. E. Kaplan, and T. M. P. Tait, J. High Energy Phys. 02 (2004) 043; 06 (2004) 032; A. Maloney, A. Pierce, and J. G. Wacker, hep-ph/0409127.

[16] R. Harnik, G. D. Kribs, D. T. Larson, and H. Murayama, Phys. Rev. D **70**, 015002 (2004); S. Chang, C. Kilic, and R. Mahbubani, Phys. Rev. D **71**, 015003 (2005); A. Birkedal, Z. Chacko, and Y. Nomura, Phys. Rev. D **71**, 015006 (2005); A. Delgado and T. M. P. Tait, J. High Energy Phys. 07 (2005) 023.

[17] T. Kobayashi and H. Terao, J. High Energy Phys. 07 (2004) 026; T. Kobayashi, H. Nakano, and H. Terao, Phys. Rev. D **71**, 115009 (2005).

[18] Z. Chacko, Y. Nomura, and D. Tucker-Smith, Nucl. Phys. **B725**, 207 (2005); Y. Nomura and B. Tweedie, Phys. Rev. D **72**, 015006 (2005).

[19] R. Dermisek and J. F. Gunion, Phys. Rev. Lett. **95**, 041801 (2005); hep-ph/0510322; S. Chang, P. J. Fox, and N. Weiner, hep-ph/0511250; P. C. Schuster and N. Toro, hep-ph/0512189.

[20] Y. Nomura, D. Poland, and B. Tweedie, hep-ph/0509243; hep-ph/0509244.

[21] A. Birkedal, Z. Chacko, and M. K. Gaillard, J. High Energy Phys. 10 (2004) 036; P. H. Chankowski, A. Falkowski, S. Pokorski, and J. Wagner, Phys. Lett. B **598**, 252 (2004); Z. Berezhiani, P. H. Chankowski, A. Falkowski, and S. Pokorski, Phys. Rev. Lett. **96**, 031801 (2006); T. Roy and M. Schmaltz, J. High Energy Phys. 01 (2006) 149; C. Csaki, G. Marandella, Y. Shirman, and A. Strumia, Phys. Rev. D **73**, 035006 (2006).

[22] R. Dermisek and H. D. Kim, hep-ph/0601036.

[23] R. Barate *et al.* (ALEPH Collaboration), Phys. Lett. B **565**, 61 (2003); LEP Higgs Working Group Collaboration, hep-ex/0107030.

[24] Y. Okada, M. Yamaguchi, and T. Yanagida, Prog. Theor. Phys. **85**, 1 (1991); J. R. Ellis, G. Ridolfi, and F. Zwirner, Phys. Lett. B **257**, 83 (1991); H. E. Haber and R. Hempfling, Phys. Rev. Lett. **66**, 1815 (1991).

[25] CDF Collaboration, D0 Collaboration, and Tevatron Electroweak Working Group, hep-ex/0507091.

[26] S. Heinemeyer, W. Hollik, and G. Weiglein, Comput. Phys. Commun. **124**, 76 (2000); Eur. Phys. J. C **9**, 343 (1999).

[27] M. Carena, M. Quiros, and C. E. M. Wagner, Nucl. Phys. **B461**, 407 (1996); H. E. Haber, R. Hempfling, and A. H. Hoang, Z. Phys. C **75**, 539 (1997).

[28] A. Djouadi, J. L. Kneur, and G. Moultaka, hep-ph/0211331.

[29] P. Skands *et al.*, J. High Energy Phys. 07 (2004) 036.

[30] L. Giusti, A. Romanino, and A. Strumia, Nucl. Phys. **B550**, 3 (1999).

[31] A. H. Chamseddine, R. Arnowitt, and P. Nath, Phys. Rev. Lett. **49**, 970 (1982); R. Barbieri, S. Ferrara, and C. A. Savoy, Phys. Lett. **119B**, 343 (1982); L. J. Hall, J. Lykken, and S. Weinberg, Phys. Rev. D **27**, 2359 (1983).

[32] R. Barbieri and G. F. Giudice, Nucl. Phys. **B306**, 63 (1988); G. W. Anderson and D. J. Castano, Phys. Lett. B **347**, 300 (1995); Z. Chacko, Y. Nomura, and D. Tucker-Smith, in Ref. [18].

[33] L. J. Hall and Y. Nomura, Phys. Rev. D **64**, 055003 (2001).

[34] M. Dine and W. Fischler, Phys. Lett. **110B**, 227 (1982); Nucl. Phys. **B204**, 346 (1982); L. Alvarez-Gaume, M. Claudson, and M. B. Wise, Nucl. Phys. **B207**, 96 (1982); S. Dimopoulos and S. Raby, Nucl. Phys. **B219**, 479 (1983).

[35] M. Dine, A. E. Nelson, and Y. Shirman, Phys. Rev. D **51**, 1362 (1995); M. Dine, A. E. Nelson, Y. Nir, and Y. Shirman, Phys. Rev. D **53**, 2658 (1996).

[36] M. A. Luty, Phys. Rev. D **57**, 1531 (1998); A. G. Cohen, D. B. Kaplan, and A. E. Nelson, Phys. Lett. B **412**, 301 (1997).

[37] For earlier work, I. Antoniadis, Phys. Lett. B **246**, 377 (1990).

[38] A. Pomarol and M. Quiros, Phys. Lett. B **438**, 255 (1998); I. Antoniadis, S. Dimopoulos, A. Pomarol, and M. Quiros, Nucl. Phys. **B544**, 503 (1999); A. Delgado, A. Pomarol, and M. Quiros, Phys. Rev. D **60**, 095008 (1999).

[39] R. Barbieri, L. J. Hall, and Y. Nomura, Phys. Rev. D **63**, 105007 (2001); N. Arkani-Hamed, L. J. Hall, Y. Nomura, D. R. Smith, and N. Weiner, Nucl. Phys. **B605**, 81 (2001).

[40] R. Barbieri, L. J. Hall, and Y. Nomura, Nucl. Phys. **B624**, 63 (2002); Phys. Rev. D **66**, 045025 (2002).

[41] R. Barbieri, L. J. Hall, G. Marandella, Y. Nomura, T. Okui, S. J. Oliver, and M. Papucci, Nucl. Phys. **B663**, 141 (2003); D. Marti and A. Pomarol, Phys. Rev. D **66**, 125005 (2002).

[42] D. Marti and A. Pomarol, Phys. Rev. D **64**, 105025 (2001); D. E. Kaplan and N. Weiner, hep-ph/0108001; G. von Gersdorff and M. Quiros, Phys. Rev. D **65**, 064016 (2002).

[43] S. Dimopoulos and H. Georgi, Nucl. Phys. **B193**, 150 (1981); N. Sakai, Z. Phys. C **11**, 153 (1981); S. Dimopoulos, S. Raby, and F. Wilczek, Phys. Rev. D **24**, 1681 (1981).

[44] R. Barbieri and A. Strumia, hep-ph/0007265.

[45] L. E. Ibanez and D. Lust, Nucl. Phys. **B382**, 305 (1992); B. de Carlos, J. A. Casas, and C. Munoz, Phys. Lett. B **299**, 234 (1993); V. S. Kaplunovsky and J. Louis, Phys. Lett. B **306**, 269 (1993); A. Brignole, L. E. Ibanez, and C. Munoz, Nucl. Phys. **B422**, 125 (1994); **B436**, 747(E) (1995).

[46] L. Randall and R. Sundrum, Nucl. Phys. **B557**, 79 (1999); G. F. Giudice, M. A. Luty, H. Murayama, and R. Rattazzi, J. High Energy Phys. 12 (1998) 027.

[47] K. Choi, A. Falkowski, H. P. Nilles, M. Olechowski, and S. Pokorski, J. High Energy Phys. 11 (2004) 076; K. Choi, A. Falkowski, H. P. Nilles, and M. Olechowski, Nucl. Phys. **B718**, 113 (2005).

[48] K. Choi, K. S. Jeong, and K. i. Okumura, J. High Energy Phys. 09 (2005) 039.

[49] M. Endo, M. Yamaguchi, and K. Yoshioka, Phys. Rev. D **72**, 015004 (2005).

[50] A. Falkowski, O. Lebedev, and Y. Mambrini, J. High Energy Phys. 11 (2005) 034.

[51] See, for example, G. C. Cho and K. Hagiwara, Nucl. Phys. **B574**, 623 (2000).

[52] R. Kitano, T. Moroi, and S. f. Su, J. High Energy Phys. 12 (2002) 011.

[53] T. Moroi and L. Randall, Nucl. Phys. **B570**, 455 (2000); M. Fujii and K. Hamaguchi, Phys. Lett. B **525**, 143 (2002); Phys. Rev. D **66**, 083501 (2002); K. Kohri, M. Yamaguchi, and J. Yokoyama, Phys. Rev. D **72**, 083510 (2005).

[54] H. Baer, K. Hagiwara, and X. Tata, Phys. Rev. D **35**, 1598 (1987); H. Baer and X. Tata, Phys. Rev. D **47**, 2739 (1993); J. L. Lopez, D. V. Nanopoulos, X. Wang, and A. Zichichi, Phys. Rev. D **48**, 2062 (1993); H. Baer, C. Kao, and X. Tata, Phys. Rev. D **48**, 5175 (1993).

[55] H. Baer, C. h. Chen, F. Paige, and X. Tata, Phys. Rev. D **50**, 4508 (1994); H. Baer, C. h. Chen, C. Kao, and X. Tata, Phys. Rev. D **52**, 1565 (1995); S. Mrenna, G. L. Kane, G. D. Kribs, and J. D. Wells, Phys. Rev. D **53**, 1168 (1996).

[56] M. M. Nojiri and Y. Yamada, Phys. Rev. D **60**, 015006 (1999); M. Drees, Y. G. Kim, M. M. Nojiri, D. Toya, K. Hasuko, and T. Kobayashi, Phys. Rev. D **63**, 035008 (2001).

[57] S. Y. Choi, B. C. Chung, J. Kalinowski, Y. G. Kim, and K. Rolbiecki, hep-ph/0504122.

[58] L. J. Hall and L. Randall, Nucl. Phys. **B352**, 289 (1991); M. Dine and D. MacIntire, Phys. Rev. D **46**, 2594 (1992); P. J. Fox, A. E. Nelson, and N. Weiner, J. High Energy Phys. 08 (2002) 035.

[59] T. Sjostrand, P. Eden, C. Friberg, L. Lonnblad, G. Miu, S. Mrenna, and E. Norrbin, Comput. Phys. Commun. **135**, 238 (2001); T. Sjostrand, L. Lonnblad, S. Mrenna, and P. Skands, hep-ph/0308153.

[60] M. Muhlleitner, A. Djouadi, and Y. Mambrini, Comput. Phys. Commun. **168**, 46 (2005).

[61] E. Richter-Was, hep-ph/0207355.

[62] E. Richter-Was, D. Froidevaux, and L. Poggioli, ATLAS Internal Note Report No. ATL-PHYS-98-131.

[63] C. G. Lester and D. J. Summers, Phys. Lett. B **463**, 99 (1999).

[64] D. R. Tovey, Phys. Lett. B **498**, 1 (2001).

[65] J. Hisano, K. Kawagoe, R. Kitano, and M. M. Nojiri, Phys. Rev. D **66**, 115004 (2002); J. Hisano, K. Kawagoe, and M. M. Nojiri, Phys. Rev. D **68**, 035007 (2003).

[66] N. Arkani-Hamed, G. F. Giudice, M. A. Luty, and R. Rattazzi, Phys. Rev. D **58**, 115005 (1998).

[67] I. Jack and D. R. T. Jones, Phys. Lett. B **473**, 102 (2000).